AD-A237 290

(2)

REPORT DOCUMENTATION PAGE

1b RESTRICTIVE MARKINGS	NONE
3 DISTRIBUTION/AVAILABILITY OF REPORT	Approved for public release. Distribution unlimited.
2b DECLASSIFICATION/DOWNGRADING SCHEDULE	
4 PERFORMING ORGANIZATION REPORT NUMBER(S)	Technical Report No. 32
5 MONITORING ORGANIZATION REPORT NUMBER(S)	
6a NAME OF PERFORMING ORGANIZATION	Massachusetts Institute of Technology
6b OFFICE SYMBOL (If applicable)	
7a NAME OF MONITORING ORGANIZATION	ONR
6c. ADDRESS (City, State, and ZIP Code)	77 Massachusetts Avenue, Room 1-306, Cambridge, MA 02139
7b. ADDRESS (City, State, and ZIP Code)	800 North Quincy Street, Arlington, VA 22217
8a. NAME OF FUNDING/SPONSORING ORGANIZATION	DARPA
8b OFFICE SYMBOL (If applicable)	
9 PROCUREMENT INSTRUMENT IDENTIFICATION NUMBER	N00014-86-K-0768
8c. ADDRESS (City, State, and ZIP Code)	1400 Wilson Boulevard, Arlington, VA 22209

10 SOURCE OF FUNDING NUMBERS

PROGRAM ELEMENT NO.	PROJECT NO	TASK NO	WORK UNIT ACCESSION NO.
R & T Code	A 400005		

11 TITLE (Include Security Classification)
Inelastic Deformation and Fracture of Glassy Solids

12 PERSONAL AUTHOR(S)
A. S. Argon

13a. TYPE OF REPORT	13b TIME COVERED	14 DATE OF REPORT (Year, Month, Day)	15 PAGE COUNT
Interim Technical	FROM 1990 TO 1991	1991 May 31	71

16 SUPPLEMENTARY NOTATION
Chapter in Vol 6 of "Materials Science and Technology" (VCH Publishing, Germany) edited by R. Cahn et al

17 COSATI CODES

FIELD	GROUP	SUB-GROUP

18 SUBJECT TERMS (Continue on reverse if necessary and identify by block number)
Glassy solids, inelastic deformation, fracture

19 ABSTRACT (Continue on reverse if necessary and identify by block number)

A general unified treatment of the phenomeriology and mechanisms of inelastic deformation in glassy media, ranging from polymers to metals to ceramics.

20 DISTRIBUTION/AVAILABILITY OF ABSTRACT	☒ UNCLASSIFIED/UNLIMITED ☐ SAME AS RPT ☐ DTIC USERS
21 ABSTRACT SECURITY CLASSIFICATION	Unclassified
22a NAME OF RESPONSIBLE INDIVIDUAL	Dr. Kenneth Wynne
22b TELEPHONE (Include Area Code)	703/696-4100
22c OFFICE SYMBOL	

11 Inelastic Deformation and Fracture of Glassy Solids

A. S. Argon

Massachusetts Institute of Technology
Cambridge, MA
U.S.A.

List of Symbols and Abbreviations

B_i	diagonal element of back-stress tensor
C_1, C_2	material constants in craze initiation model
E	Young's modulus
ΔE	Potential energy barrier for segment rotation
ΔF	Helmholtz free energy
ΔF_v	Helmholtz free energy barrier for viscous flow
G_I	Mode I energy release rate
ΔG	Gibbs free energy
ΔG_0	Scaling constant for Gibbs free energy
ΔG^*	Gibbs free energy of activation
J	polar moment of inertia of atom group
K_I	Mode I stress intensity factor
M_e	entanglement molecular weight
Q	material constant in craze initiation model
R	universal gas constant, also reaction rate constant in Eqns (11.9c and 11.29)
R_p	plastic zone size
T	absolute temperature

Y tensile yield strength

a molecular radius, also crack half length in Eqns. (11.30 and 11.32), also curvature of local intermolecular energy in ring rotation in Eqn. (11.28)

b interatomic distance

c volume fraction

c_e volume fraction at steady state flow

d_i component of shear direction vector

h pri-mordial thickness of craze material

k Boltzmann's constant

m stress exponent

n_i component of unit normal vector of shear plane

p numerical constant

q numerical constant

r_{ij} magnitude of vector connecting atoms i and j

s deviatoric shear stress (a scalar quantity)

s_{ij} element of deviatoric stress tensor

t_i craze initiation time

v_o pre-exponential craze velocity constant

v_{cb} velocity of craze border

v_{ct} velocity of craze tip

Δv^* shear activation volume

Φ pair potential energy function

Ω_o population average of volume per atom

Ω_i volume per atom at site i

Ω_f average volume per atom in a finite cluster

Ω_c volume of cluster

χ surface free energy

α a proportionality constant

α_{ij} elements of the geometrical (Schmid) resolution tensor

β dilatancy coefficient

$\dot{\gamma}$ inelastic shear strain rate

$\dot{\gamma}_o$ phenomenological shear strain rate scaling factor

$\dot{\gamma}_G$ pre-exponential factor of strain rate

δ increment

ϵ uniaxial strain

ϵ_{ij}	element of strain tensor
ϵ^T	unconstrained uniaxial transformation strain
γ^T	unconstrained transformation shear strain
λ_i	principal extension ratio
λ_n	limiting extension ratio, lacking stretch
λ'	hardening-modified extension ratio
μ	shear modulus
ν	Poisson's ratio
ν_G	frequency factor
ω	molecular segment rotation angle
ρ	density
σ	applied shear stress
$\sigma_{\alpha\beta}(i)$	element of stress tensor at atomic site i
σ_m	applied mean normal stress, negative pressure
σ_{ij}	element of applied stress tensor
θ	dilatation
$\hat{\tau}$	threshold plastic shear resistance (a scalar quantity)
$\hat{\tau}_{ij}$	ideal shear strength

11.1 Introduction

Under certain conditions many solids can be obtained in a partially or completely disordered form. We are interested here in the inelastic deformation and fracture of such solids in the range of temperature in which their structure does not change substantially, i.e., below their glass transition temperature. While such solids have often been referred to as *amorphous* which implies the complete absence of structural regularity, we will prefer to call them *glassy* to accommodate possibilities of some short range or intermediate range order which is often found to be present. It must be emphasized, however, that our principal assignment will not be the description of the atomic or molecular structure of these solids beyond a certain level that is necessary to understand the mechanisms of deformation. Extensive description of the structure of glasses and the experimental tools available for their measurement can be found in Volume 9 of this series of treatises.

The subject of inelastic deformation of solids is a broad one that can not be treated adequately in its entirety in a single chapter. Therefore, here we will concentrate primarily on a discussion of the mechanisms of such deformation in nearly homogeneous solids, to large inelastic strains, under the simplest non-trivial states of stress, emphasizing the physics rather than the operational mechanics aspects of the deformation. Heterogeneities, are often important in modulating the deformation process such as in the case of partially crystalline structures where the crystallites do not undergo much deformation. They are also of great importance in fracture where they act as principal sources not only for fracture initiation but also for toughening of some brittle polymers. These topics will, however, not be developed in this chapter.

While we will pay attention to the important structural differences in the deformation mechanisms between atomic glasses (metallic glasses), network glasses (oxide glasses) and polymeric glasses that govern the local kinematics of the deformation process, we will emphasize as much as possible the common unifying features. We will concentrate our attention only on monotonic deformation and fracture rather than on the cyclic variety which has many important differences requiring extensive additional developments. Readers interested in cyclic response of engineering solids in general and also many glasses in particular are referred to Suresh (1991).

Apart from the necesity to understand the special stress and strain conditions of the crack tip environment in the development of the fracture mechanisms we will not discuss in any detail the mechanics aspects of fracture.

An elegant and crisp treatment of this subject has been given by Hutchinson (1979) to which the reader is referred.

11.2 Structure of Glasses

11.2.1 Glass Formation

Formation of glasses upon cooling from the melt relies principally on the necessity to suppress nucleation of a crystalline phase. That the nucleation and growth of crystallites from a melt, in the absence of heterogeneities, requires substantial undercooling and that the accompanying sharply reduced kinetics of diffusion or ordering makes the establishment of a crystalline phase even more difficult is common knowledge. The specific conditions required to override crystallization to form a glass in different materials, alloys, or mixtures, such as special features in the phase equilibrium diagrams, the nature of diffusion or ordering in the melt, molecular topological constraints, etc. have been widely discussed in the literature for specific glasses and will not be developed here. More extensive coverage of this subject can be found in Volumes 9 and 12 of these treatises for all types of glasses including atomic glasses, network glasses and chain polymeric glasses.

11.2.2 Atomic Structure of Glasses

11.2.2.1 Relation of Structure to Deformation Mechanisms

The mechanisms of inelastic deformation by motion of dislocations, transport of point defects, or by twinning or martensitic shear transformations in crystalline solids are well understood because of the clear connection between the regular crystal structure and the relatively simple kinematics of the atomic motions that are involved. In comparison with this the detailed understanding of the mechanisms of inelastic deformation in glasses and the specific kinematics of atom motions that are involved are far less clear. This is a direct result of the difficulty of accurately describing the structure of glasses, and those regions in them that are most favorably endowed for the local atomic motions that produce inelastic strain. Most, if not all, experimental probes of the structure of glasses only provide information on the volume averaged features of the structure which can not uniquely distinguish

between different forms of aggregation of atoms associated with variations of local packing, some forms of short range order, and even more importantly, between different forms of relative spatial correlation of the extreme portions of the spectrum of structural disorder (Ziman, 1979; Gaskell, 1983). While these spatial variations of disorder and their correlation has often little influence on the overall volume averaged physical properties, they are of overwhelming importance for the understanding of inelastic deformation (and parenthetically, also of diffusion). It is for this reason that computer simulations of the structure and the associated mechanisms of inelastic deformation of glasses of all types have been very informative as we will discuss below.

11.2.2.2 Radial Distribution Functions

A characteristic form of structural information obtained from x-ray or neutron diffraction experiments is the radical distribution function (RDF) of atom positions around a typical atomic site (see Ziman, 1979). Such RDF's provide useful information on the distribution of volume averaged coordination of atoms in the glassy state, and give a useful visual diagnostic means of gauging the average degree of disorder from the shapes of these functions. The RDF's, however, are not a sensitive indicator of the local correlations of disordered material of different description. Thus, their utility in understanding inelastic deformation is limited. They serve, nevertheless, as a convenient bridge in connecting results of structural simulations to experimental information, where the information provided by the simulation furnishes a degree of specificity often not reflected in the experimental results.

11.2.2.3 Distributions of Atomic Packing or Interstitial Sites

Bernal (1964) has pioneered the analysis of dense random packed ball bearing spheres as analogs for the structure of simple liquids, and by extension, that of atomic glasses, demonstrating that the disordered structure of such assemblages of hard spheres can be described by a certain distribution of five different polyhedral figures which characterize interstitial space in these assemblages. The exercise was repeated computationally by others. Frost (1983) has determined that characterization of the disordered space made up from dense random packing of spheres by means of polyhedral figures having atom sites at their apexes requires more than the five canonical figures

identified by Bernal. He proceeded further and also furnished distributions of sphere sizes that can just fit into interstitial holes. This latter information is of interest in understanding sorption and diffusion of gases.

An alternative representation of tesselation of space is by *Voronoi* polyhedra constructed around atoms rather than interstitial sites. This was studied first by Finney (1970a) and subsequently by others. It provides information on the distribution of the volume per atom. Figure 11.1 gives such a distribution of volume per atom in a dense random packing of hard spheres in units of the average atomic volume in the glass. The distribution shows that while the average volume per atom is only about 9% larger than that in the reference crystal there is a considerable tail of larger volumes, which as we will see play an important role in inelastic deformation. Simulations using actual interatomic interaction potentials rather than hard spheres have given very similar results (Finney, 1970b).

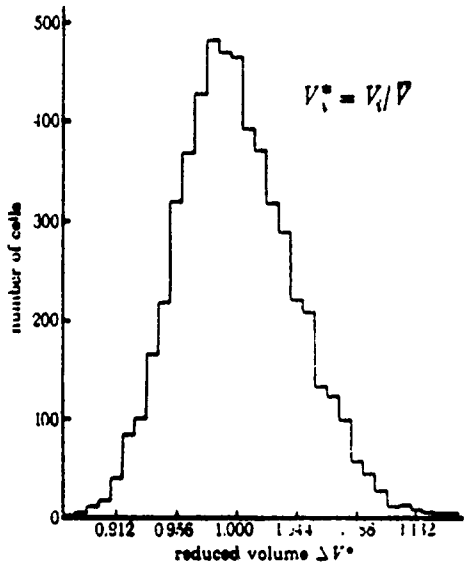

Figure 1: Figure 11.1: Distribution of volume per atom in an atomic packing model (Finney, 1970a).

While the atomic packing studies in 3-D should be clearly preferred to compare with experimentally obtained diffraction information, the visualization of such packing, and the forms of its alteration upon deformation is often difficult to achieve. For this reason several 2-D models have also been studied in considerable detail. One of these is a disordered variant of the well

known Bragg bubble model making use of the capillary inter-bubble forces acting between small soap bubbles floating on the surface of water (Argon and Kuo, 1979). The behavior of such rafts upon deformation in the plane of the raft have given considerable insight into the nature of plastic flow (Argon and Shi, 1982).

11.2.2.4 Free Volume:

That excess atomic volume concentrated into local regions in a disordered solid may permit relatively easy rearrangements there has been recognized for a long time and has been associated with the notion of free volume. While the notion is often loosely used to advance qualitative arguments, it can be made more precise into a structure characterizing parameter in the computer simulation models. There it has been defined as (Deng et al, 1989b)

$$\Omega_f = \frac{1}{n}\sum_{i=1}^{n}(\Omega_i - \Omega_0) \tag{11.1}$$

where Ω_f is the average excess volume per atom in a cluster of n atoms, over the population average volume Ω_0 per atom. Theoretical considerations (Cohen and Grest, 1979) and computer simulations (Deng et al, 1989a,b) have indicated that regions in which such excess volume clusters, i.e., where free volume aggregates, show a reduced level of local elastic stiffness or reduced cohesion, and have so-called liquid-like behavior. Topological evidence suggests that in the melt, and even in the sub-cooled melt regime, above the glass transition temperature (T_g), overall compliant behavior results from the percolation of liquid-like material through the structure. Below T_g this percolation is broken and the material exhibits overall stiff behavior as now the relatively more densely packed stiff material becomes contiguously connected (Deng et al, 1989a,b). In Section 11.4.2 we will furnish evidence that the liquid-like material that is spatially isolated below T_g nevertheless constitutes the fertile material in which plastic rearrangements preferentially occur (Deng et al, 1989d).

11.2.2.5 Packing of Atoms in Network Glasses and Chain Polymeric Solids

The structures obtained from dense random packed spheres are of great value in elucidating complex topological concepts, and also serve as idealized

models of the structure of glassy metals where the idealization has merit. In space network glasses such as fused SiO_2 and its many modifications, as well as in chain polymeric glasses the structures must be simulated by the use of the appropriate interatomic force fields between bonded atoms as well as non-bonded atoms. Such simulations have also been performed for many systems. The results of these simulations are best discussed in the context of the deformation studies for which they have been developed. Therefore, we postpone their introduction to Sections 11.5 and 11.6

11.2.2.6 Atomic Site Stress Tensor

The glassy state has been associated with excess enthalpy which has been useful in understanding calorimetric measures of structural relaxation. Such average scalar measures of the excess properties of the glass, however, do not convey much information on where the local excess properties congregate, or more importantly, where and how the mechanical response occurs. For such purposes, Egami and Vitek (1983) have emphasized the utility of the atomic site stress tensor defined much earlier by Born and Huang (1954) on the local application of the virtual work principal at each atomic site based on the level of equilibrated forces acting on individual atoms. For atomic solids, where substantially only central forces act between atoms, the atomic site stress tensor is defined as

$$\sigma_{\alpha\beta}(i) = \frac{1}{2\Omega_i} \sum_{j \neq i} \left[\frac{\partial \Phi(r)}{\partial r} \right]_{r=r_{ij}} \frac{r_{ij}^{\alpha} r_{ij}^{\beta}}{r_{ij}} \tag{11.2}$$

where Φ is the interatomic pair potential from which all interatomic forces are calculated, r_{ij} is the magnitude of the radius vector connecting atoms i and j, r_{ij}^{α} and r_{ij}^{β} are the magnitudes of the α and β components of the radius vector connecting atoms i and j and Ω_i is the volume of the central atom i for which the tensor component is defined. The sum is over all j neighbors with which atom i is effectively interacting. Egami and Vitek have calculated the distribution of the two scalar invariants of the atomic site stress tensors: i.e., the mean normal stress σ_m (negative pressure) and the deviatoric (Mises) shear stress for a specific simulation. Their results, given in Figs. 11.2(a) and 11.2(b) show that the rms value of the mean normal stress is 6% of the bulk modulus, while that for the deviatoric shear stress is fully 18% of the shear modulus. These magnitudes border on the cohesive resistances of the solid and are very substantial. Egami and Vitek (1983)

have proceeded further and have demonstrated that it is possible to account for the excess enthalpy of the glassy state by considering the elastic strain energies associated with the atomic site stresses in the glass – in reference to those in the ordered crystalline phase of the material. We will demonstrate in Sections 11.4.2 and 11.6.3 the general utility of the atomic site stress tensor in the computational simulations of plastic resistance in metallic and polymeric glasses respectively.

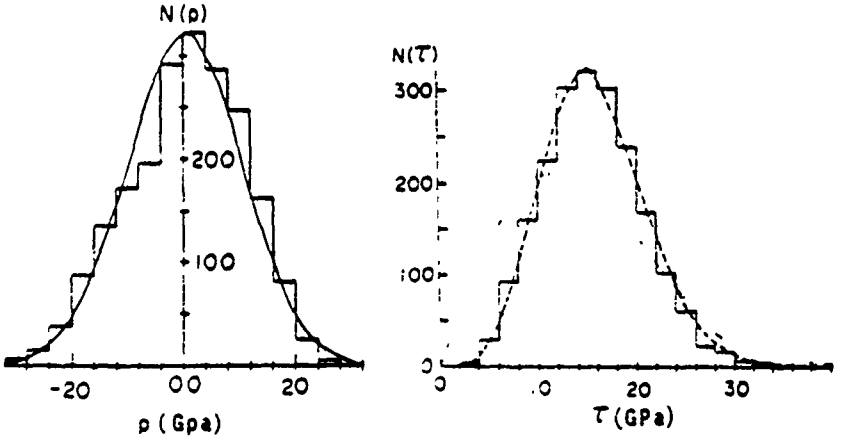

Figure 2: Figure 11.2: Distribution of atomic site stresses: (a) negative pressure; (b) deviatoric shear stress (Egami and Vitek, 1983).

11.2.2.7 Other Topological Characterizations of the Glassy State

In addition to the forms of structural characterization described above there have been many attempts in the nature of abstract topological transformations to find a unique connection between a characteristic disordered state of the glass and a reference ordered state. While many of these studies stand out as ingenious, they have so far failed to provide much help in better understanding of local inelastic rearrangements. The interested reader will find a good selection of these models presented by Vitek (1983).

11.3 Overview of Phenomenology, Mechanics and Mechanisms of Inelastic Deformation and Fracture of Glasses

11.3.1 Phenomenological Conditions for Inelastic Deformation

Inelastic deformation in solids is a rate process which, in the limit of very low temperatures, requires for its initiation a critical deviatoric shear stress to overcome a threshold shear resistance $\hat{\tau}$ which for a given state of the solid, is a material property. Thus as $T \rightarrow 0$, plasticity is initiated when

$$s = (s_{ij}s_{ij}/2)^{\frac{1}{2}} = \hat{\tau}(\sigma_m) \tag{11.3}$$

where $s_{ij} = \sigma_{ij} - \sigma_m$ are the so-called deviatoric stresses, $\sigma_m = \sigma_{ii}/3$ is the mean normal stress, and repeated indices imply summation over all indices $i = 1, 2, 3$ etc. Equation (11.3) indicates that the threshold plastic resistance $\hat{\tau}$ may depend on σ_m. Under these conditions the plastic strain rate $\dot{\gamma}$ is arbitrarily high. At higher temperatures, but still well below T_g where the structure does not undergo significant relaxation during the time of deformation, the plastic strain rate should be given by (Kocks et al, 1975).

$$\dot{\gamma} = \dot{\gamma}_G \exp(-\frac{\Delta G^*(s/\hat{\tau})}{kT}) \tag{11.4}$$

where the stress dependence of the activation free energy ΔG^* of the deformation process can be often expressed phenomenologically as

$$\Delta G^* = \Delta G_0(1 - (\frac{s}{\hat{\tau}})^p)^q. \tag{11.5}$$

where p and q are exponents close to unity.

The pre-exponential factor of the rate expression $\dot{\gamma}_G$ combines a fundamental frequency factor ν_G of the deformation producing unit, the local plastic transformation strain increment γ^T and the volume fraction c of deformation units, i.e.,

$$\dot{\gamma}_k \approx c\gamma^T \nu_G. \tag{11.6}$$

The mechanism inspired form of the strain rate expression given in Eqn (11.4) can often be phenomenologically restated as a power-law form

$$\dot{\gamma} = \dot{\gamma}_0(\frac{s}{\hat{\tau}})^m \tag{11.7}$$

where both $\dot{\gamma}_0$ and m are fitting constants. Equation (11.7), albeit more approximate, incorporates a reverse deformation component that is left out in Eqn (11.4), which permits the strain rate goes to zero when $s \rightarrow 0$, at least formally. More specific forms of these expressions will be discussed below.

In many mechanistic models only an applied shear stress σ is considered, so that $s \rightarrow \sigma$.

11.3.2 Kinematics of Inelastic Strain

11.3.2.1 Distortional Plasticity

There has been much controversy associated with the mechanism responsible for plastic strain production and its kinematics in glassy solids. Since a number of glassy metals and polymers exhibit strong shear localization, it was proposed first by Gilman (1968), and then by many others, that plastic deformation in these solids is produced by generalized dislocations having similar mobility characteristics as those in metal crystals. While there is considerable merit in considering dislocations for operational purposes of local stress analysis or accounting for the macroscopic strains, there is no firm evidence that there is any analogous mobile defect in a glassy solid resembling a crystal dislocation (Argon, 1981). Instead, much evidence based on computer simulations indicates that shear is produced in glassy solids by means of individual shear transformations occurring in small atom clusters which do not propagate in a contiguous manner outward from the initial cluster. Thus, mechanistically the rate process of plastic deformation appears to be nucleation controlled rather than controlled by the mobility of the boundaries of the transformation.

If such shear transformations can be considered to have shapes of oblate spheroids with principal axes characterized by unit normal sectors $\vec{d}$ and $\vec{n}$ in the plane and out of the plane of the transformation shear increment γ^T, as shown in Fig. 11.3, the resulting macroscopic plastic strain increment $\delta\epsilon_{ij}$ is

$$\delta\epsilon_{ij} = \delta(c\gamma)^T \alpha_{,} \tag{11.8}$$

$$\alpha_{ij} = \frac{1}{2}(d_i n_j - d_j n_i) \tag{11.8a}$$

In Eqn (11.8) α_{ij} are elements of a geometrical (Schmid) shear strain resolution tensor relating the local shear strain increment in the spheroid coordinates to the external shape coordinates, and c is the volume fraction of the local material undergoing the transformation. Since the structure of a glass tends to be isotropic down to rather small volume elements, the shapes of the local shear transformations can be expected to be relatively equiaxed, with

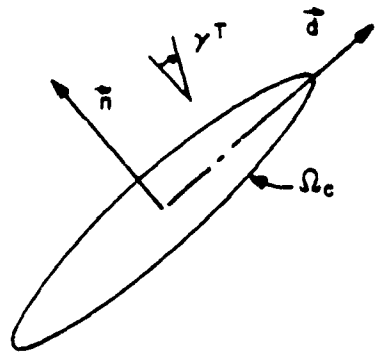

Figure 3: Figure 11.3: Principal directions of ellipsoidal shear transformation: $\vec{n}$ is unit normal vector of invariant plane, $\vec{d}$ is parallel to shear direction.

the directions of the local shear axes coinciding with those of the macroscopic body. Thus, giving

$$\delta\gamma = \delta(c\gamma^T). \tag{11.8b}$$

For a longer-term average point of view that considers the formation of the transformations as "instantaneous", where γ^T must be considered as a property of the structure, then

$$\delta(c\gamma^T) = \gamma^T \delta c. \tag{11.8c}$$

Equations (11.8 a-c) are in incremental form. They can be extended into rate form when they transform into

$$\dot{\epsilon}_{ij} = \alpha_{ij}\frac{d}{dt}(c\gamma^T) \rightarrow c_s\gamma^T\alpha_{ij}R \tag{11.9a}$$

$$\dot{\gamma} = c_s\gamma^T R, \tag{11.9b}$$

where c_s is now a steady state volume fraction of fertile material available to transform, and that the rate of transformation is governed by a stress and temperature dependent exponential Arrhenius rate constant R such as that appearing in Eqn. (11.4), i.e.,

$$R = v_G \exp(-\frac{\Delta G^*(s/\hat{\tau})}{kT}). \tag{11.9c}$$

The form of the expressions (11.9 a-c) implies that a kinematical steady state exists among volume elements so that the transformable (fertile) fraction of

material is never exhausted.

11.3.2.2 Dilatational Plasticity

Under certain conditions the plastically deforming solid can undergo stable cavitation homogeneously or in planar zones. This produces additional strain of a dilatational nature. A prominent example of this is the crazing phenomenon in certain flexible chain glassy polymers where a primordial slab of polymer becomes fibrillar or spongy, normal to the principal tensile stress as shown in Fig. 11.4. This effectively results in a dilatational transformation associated with a tensile transformation strain ϵ^T in the primordial slab. The overall tensile strain increment then, in the direction of the tensile stress is

$$\delta\epsilon = \delta(c\epsilon^T) = \epsilon^T \delta c, \tag{11.10}$$

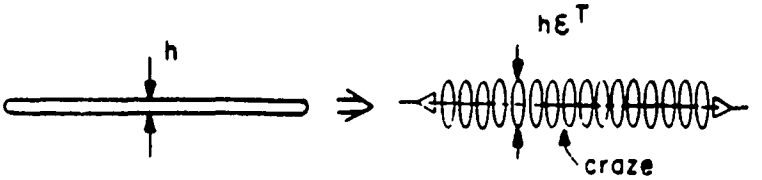

Figure 4: Figure 11.4: Craze as a dilatational transformation.

where δc is the increment in the volume fraction of the initial primordial material undergoing the crazing expansion. Since inside the craze there are no associated other transverse strains, the uniaxial strain of Eqn. (11.10) is also the net dilatation increment $\delta\theta$, in the body, i.e.,

$$\delta\theta = \delta\epsilon. \tag{11.11}$$

11.3.3 Plasticity vs Brittle Behavior

Because plastic flow in glassy solids is primarily initiation controlled, it occurs at relatively high stresses in relation to the cohesive properties of the solid. Therefore, fracture is usually a close competitor to plastic flow – particularly when it occurs in a tensile field. The choice in the terminal mechanical behavior of solids in tension, between inherent brittleness and inherent plasticity rests with the nature of the atomic bond. In two complementary fundamental developments Kelly et al (1967) and Rice and Thomson (1974) have stated that this bifurcation in behavior is governed in the limit at the tip of an atomically sharp crack. These. concentrated tensile stresses ahead of the crack probe the ideal cohesive strength of the solid while the maximum concentrated shear stresses on some inclined planes probe the ideal shear strength. Upon stressing the cracked solid, brittle vs ductile behavior is governed by whether or not the conditions of decohesion in the plane of the crack are reached before the conditions of ideal shear. In the covalently bonded network glasses the balance appears to be tilted clearly in the direction of brittleness in tension while for metallic and polymeric glasses the tilt is toward plastic behavior, for these glasses in the unaged form (Argon, 1982). As we will discuss somewhat more extensively in Section 11.7.1 the bifurcation in the behavior of metallic and polymeric glasses, however, depends strongly on the state of structural aging in these materials which produces changes in plastic resistance. Here it should suffice to state that plastic response in a glass is always attainable in principle, but may in specific instances require suppression of fracture by superposition of a pressure to inactivate cracks or flaws.

11.3.4 Mechanisms of Fracture in Glasses

As in other solids, in one limit, fracture in glasses could be a process of brittle separation with no, or negligible accompanying plastic flow. Oxide glasses and many structurally aged glassy metals fracture in this mode responding locally to a critical decohesion criterion at the tip of a propagating crack that can be characterized by a critical Mode I stress intensity criterion.

In unaged metallic glasses and in most stiff chain glassy thermoplastic or thermosetting polymers fracture is a process of ductile separation. Here

the actual separation occurs in two stages. First the continuous solid is rendered discontinuous by cavity formation at heterogeneities, followed by plastic expansion of these cavities to complete local ligament rupture as illustrated in Fig. 11.5, in a manner closely resembling the ductile fracture process in crystalline metals.

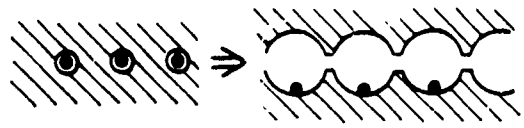

Figure 5: Figure 11.5: Formation and growth of ductile fracture cavities.

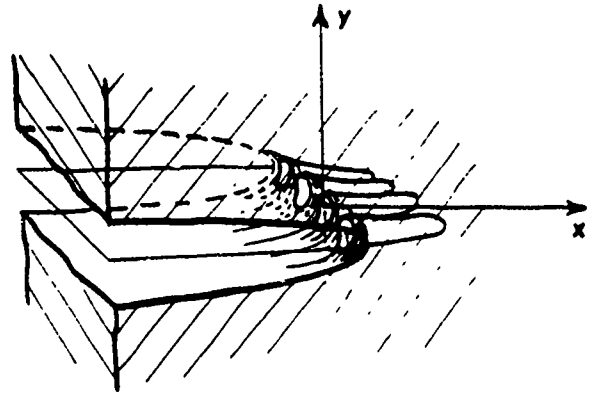

Figure 6: Figure 11.6: Sketch of break-up into fingers of ductile crack tip acting as a non-linear fluid meniscus.

Many ductile metallic glasses, free of heterogeneities, however, fracture by a variant of a fluid flow instability where the plastically blunted crack tip acts as a fluid meniscus advancing under the deformation induced negative pressure gradient zone of the blunted crack tip. The concave meniscus-like flow field becomes unstable to flow perturbations of a certain wave length which first penetrate into the crack tip zone in the from of tubular fingers followed by rupture of the ridges separating these tubular zones of penetra-

tion as sketched out in Fig. 11.6. The separation advances with the crack tip in a self-similar form of steady ductile separation.

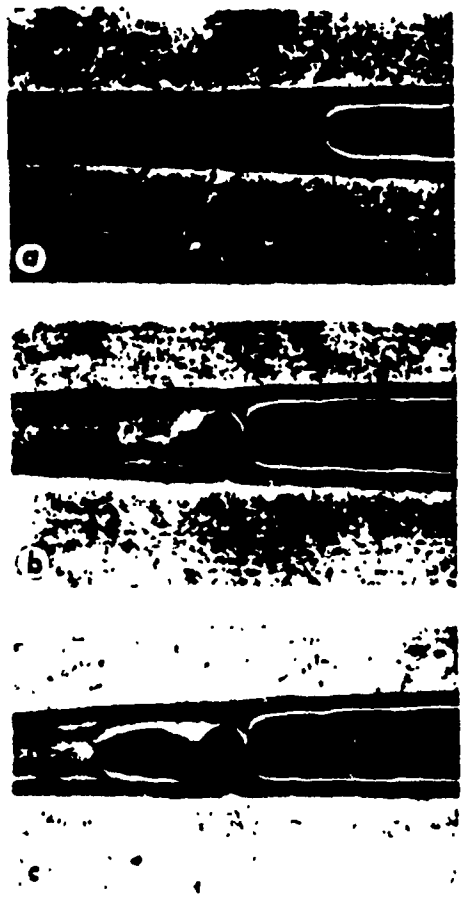

Figure 7: Figure 11.7: A sequence of fracture of a craze: (a) an advance cavitation event from a dust particle ahead of the main crack in a craze at point $P(b,c)$ the fracture spreading from the advance cavitation site joins the main crack (Doyle et al., 1972).

In flexible chain thermoplastic glassy polymers the fracture process is preceded by crazing where crazes that spread through the polymer undergo internal break-up due to intrinsic non-uniformities in the fibrillar or spongy craze matter. More often, however, crazes begin to fail from the interface of a particulate heterogeneity that the growing or widening craze acquires as shown in the sequences of states in Figs. 11.7(a)-11.7(c). Since crazes act both as ingredients promoting dilatational plasticity and also as the prominent sites of fracture, they can become an important means of controlling toughness in such glassy polymers.

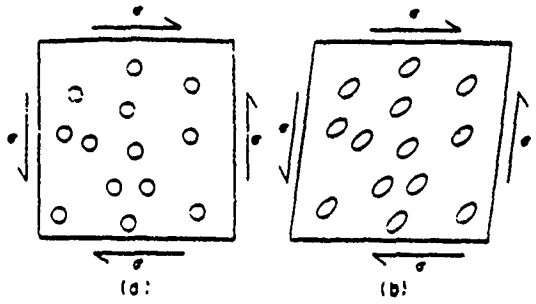

Figure 8: Figure 11.8: Sketch depicting development of shear distortion by the accumulation of isolated shear transformations under stress (Argon and Shi, 1982).

11.4 Inelastic Response in Metallic Glasses

11.4.1 Experimental Observations

11.4.1.1 Anelasticity

The distributed nature of atomic d. order in a metallic glass permit different volume elements to undergo shear relaxation under an applied stress with different ease. This can be characterized by assigning different volume elements different terminal plastic shear resistances $\hat{\tau}$ or, in an associated manner, consider them to have different activation barriers to shear transformation under a stress $\sigma \ll \hat{\tau}$. This difference can be probed best, and in the least invasive manner, by internal friction experiments. (Berry, 1978; Morito and Egami, 1984; Deng and Argon, 1986a) or by anelastic creep and creep recovery experiments (Berry, 1978; Argon and Kuo, 1980). Figure 11.8 gives a schematic representation of the response of the solid by anelastic creep where the application of a stress σ mechanically polarizes the structure by permitting the accumulation of shear relaxations that can occur at a given temperature during the period under stress. Increasing the time of observation, or increasing the temperature, increases the total strain by permitting more of the more difficult transformations to occur. In an internal friction experiment such transformations occur in the forward and reverse manner

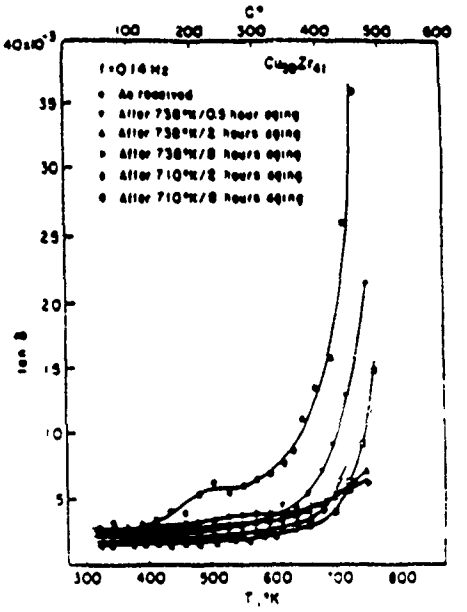

Figure 9: Figure 11.9: Change of internal friction with temperature and its dependence on aging below T_g in a Cu_{59} Zr_{41} alloy (Deng and Argon, 1986a).

and the associated hysteresis produces energy dissipation. Figure 11.9 gives a typical internal friction spectrum of the cyclic loss ($\tan\delta$) in torsional oscillations in a Cu_{59} Zr_{41} glass at different levels of aging (Deng and Argon, 1986a) while Fig. 11.10 shows the typical linear, reversible anelastic creep response of a $Pd_{80}Si_{20}$ glass at 176 C (Berry, 1978). Argon and Kuo (1980), and Deng and Argon (1986b) have demonstrated how the distribution of critical activation barriers to the local stress relaxations can be obtained from the analysis of the anelastic creep and the internal friction experiments. Figures 11.11(a) and 11.11(b) give the distributions of activation energies for transformations in $Pd_{80}Si_{20}$ and $Cu_{59}Zr_{41}$, deconvoluted from anelastic creep and recovery creep experiments, and from internal friction experiments, respectively. Figures 11.9 and 11.11(b) show that the internal friction experiment that produces nearly no permanent change in the structure during the measurement is a very sensitive method for the study of structural relaxations.

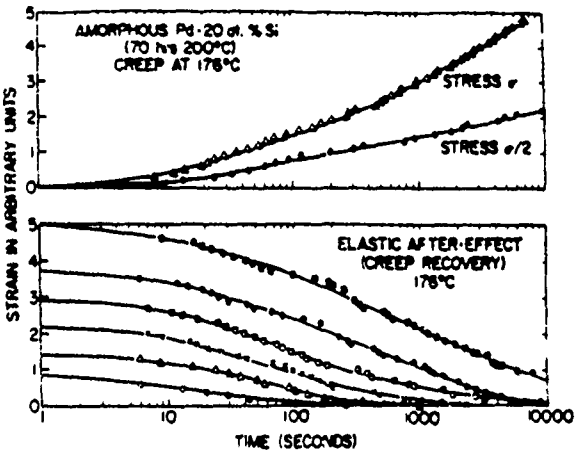

Figure 10: Figure 11.10: Linear anelastic creep and creep recovery in a $Pd_{80}Si_{20}$ glass at 176 C (Berry, 1978).

11.4.1.2 Viscous Flow

When creep experiments at low stress levels ($\sigma \ll \hat{\tau}$) are continued at higher temperatures and for longer periods of time, it is thought that the accumulating shear transformations, as sketched out in Fig. 11.8, begin to progressively fill the volume and form contiguously transformed region, percolating through the structure (Argon and Shi, 1983). This should destroy memory of the initial unstrained structure and result in a monotonically increasing component of irrecoverable viscous strain. Taub and Spaepen (1979, 1980) have used viscous flow experiments as a probe to determine the effects of structural relaxations in a $Pd_{80}Si_{20}$ glass. The temperature dependence of the viscosity of such a glass after a series of aging treatments at different temperatures is shown in Fig. 11.12. The remarkable finding is that the activation energy for the flow is unaltered by the different aging treatments but that the viscosity is systematically and dramatically increased with increasing aging temperature or increasing structural compaction. Since viscous flow is always controlled by the highest activation energies of the spectrum, i.e., the most difficult to deform component, and since the internal friction

studies show that structural relaxation primarily alters the lower end of the spectrum as shown in Fig. 11.8, these results are not unexpected. The dramatic increase in the viscosity, however, indicates also a key interdependence between different parts of the activation energy spectrum of shearing sites. The elimination of low energy sites with large free volume does not only reduce the anelastic response of the glass, but it also removes the "triggering" mechanism that permits the shear relaxation in the viscous flow of the high energy component of the spectrum. This suggests that the main effect of structural relaxation is the progressive removal of the more readily rearrangeable component of material having large free volume. This can be formally considered as a change occurring in a factor $p(\Omega_f)$ in the preexponential factor $\dot{\gamma}_G$ of the principal strain rate expression, as defined by Eqn. (11.4), where

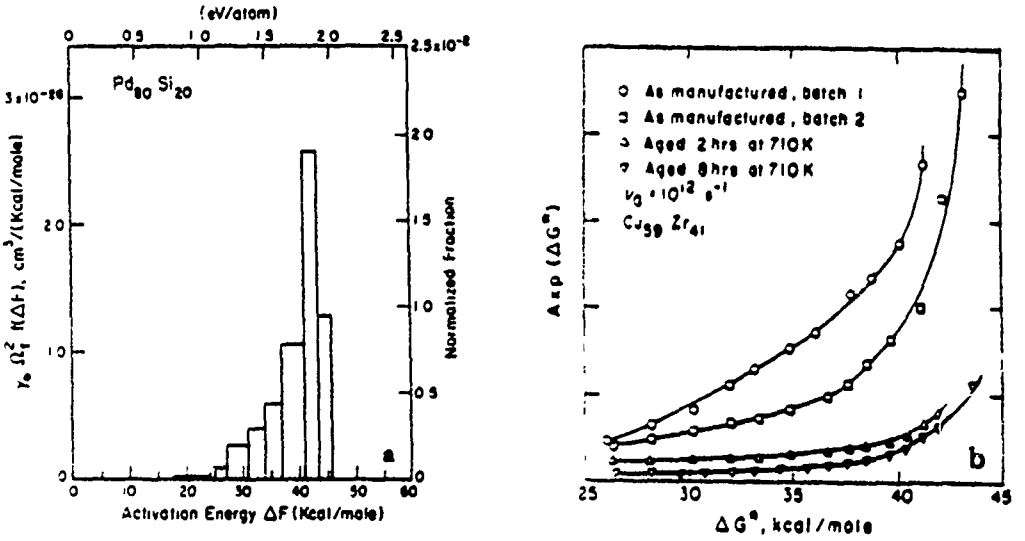

Figure 11: Figure 11.11: Distribution of activation energies for anelastic response: (a) $Pd_{80}Si_{20}$ (Argon and Kuo, 1980); (b) Cu_{59} Zr_{41} (Deng and Argon, 1986a).

$$p(\Omega_f) = \exp(-\alpha\Omega_f/\Omega_0) \tag{11.12}$$

represents the probability of finding a local region with free volume in excess of Ω_f (Argon, 1985). The computer simulations of inelastic relaxations in model glassy solids, discussed in Section 11.4.2 below are in support of this interpretation.

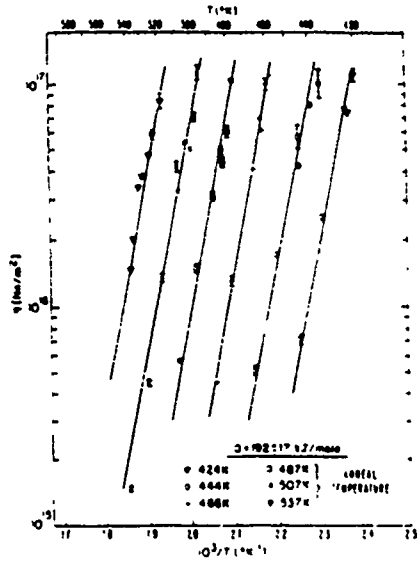

Figure 12: Figure 11.12: Dependence of shear viscosity of $Pd_{82}Si_{18}$ on temperature for different aging treatments (Taub and Spaepen, 1980).

11.4.1.3 Plastic Flow

As the applied shear stress σ becomes closer to the mechanical threshold resistance $\hat{\tau}$ the inelastic strain rate increases non-linearly with stress and tends to become asymptotically unbounded as $\sigma \rightarrow \hat{\tau}$. Alternatively upon the imposition of a relatively high strain rate of the level usually applied by laboratory testing machines, a state of plastic flow with negligible hardening behavior is reached after a more or less stretched out elastic-to-plastic transition as is shown in Fig. 11.15 for the case of a $Pd_{80}Si_{20}$ sample strained in tension (Megusar et al., 1979).

Plastic flow in metallic glasses has a number of features that are characteristic of plastic flow in crystalline metals. First, the temperature dependence of the plastic resistance is relatively small in the low temperature region, as shown for the typical case of $Pd_{80}Si_{20}$ and $Pd_{77.5}Cu_6$ $Si_{16.5}$ in Fig. 11.14. Second, the strain rate sensitivity of the plastic resistance is small, or stated alternatively, the strain rate is a very strong function of the applied stress, with a phenomenological stress exponent m of the strain rate,

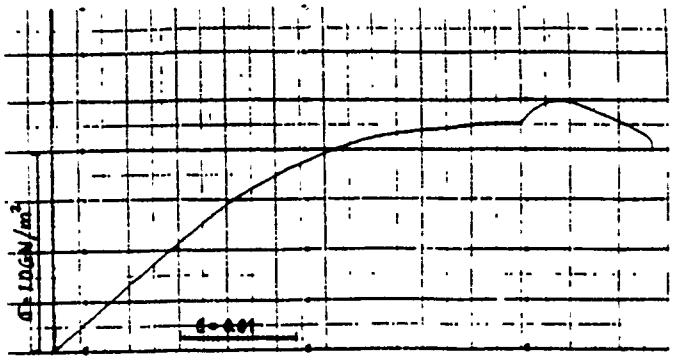

Figure 13: Figure 11.13: A stress-strain curve for $Pd_{80}Si_{20}$ at 433 K for a strain rate of $1.4 \times 10^{-5} s^{-1}$, with a sudden excursion to a strain rate of $3.4 \times 10^{-6} s^{-1}$.

as defined in Eqn. (11.7) becoming ever larger as the temperature decreases. This trend is shown in Fig. 11.15 for a $Pd_{80}Si_{20}$ glass in the relatively high temperature range near T_g where the deformation is homogeneous and conventional strain rate change experiments can be performed relatively easily. The figure shows that as $T \rightarrow T_g$ and the resistance to deformation becomes progressively smaller in comparison with $\hat{\tau}$, the behavior apparently reverts to a viscous type. The data shown in Fig. 11.15 is given also in columns 1-3 in Table 11.1, from which the usual shear activation volumes Δv^* can be determined according to the well known relations

Table 11.1 Stress Exponents m, and Activation Volumes Δv^*, Measured in Strain Rate Pd_{80} Si_{20} Change Experiments by Megusar et al (1979)

$T,(K)$	$\sigma^{\dagger}$ (GPa)	$m = d\ell n\dot{\epsilon}/d\ell n\sigma$	$\Delta v^*(m^3)$
413	1.29	11.74	8.98×10^{-29}
433	1.13	8.64	7.90
453	1.02	7.21	7.65
473	0.94	6.15	7.40
493	0.86	7.16	9.81
513	0.65	5.42	10.20
533	0.64	4.51	8.98
553	0.57	5.23	12.10

† Tensile flow stress at a strain rate of $\dot{\epsilon}_1 = 1.4 \times 10^{-5} s^{-1}$

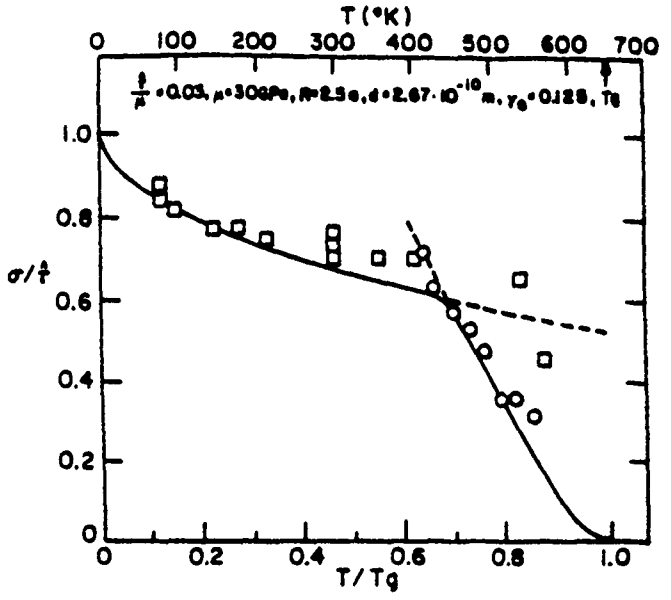

Figure 14: Figure 11.14: Dependence of the flow stress on temperature for $Pd_{80}Si_{20}$ (0) Megusar, et al, 1979); and $Pd_{77.5}Cu_6$ $Si_{16.5}$(□) (Pampillo and Chen, 1974). Solid curve is the fit obtained with the model of Section 11.4.2.

$$\Delta v^* = -(\frac{\partial \Delta G^*}{\partial \sigma})_T = kT(\frac{\partial \ell n \dot{\gamma}}{\partial \sigma})_T = kT\frac{m}{\sigma}. \qquad (11.13)$$

These are listed in column 4 of Table 11.1 and apart from some scatter, appears to be constant at a level of about $\Delta v^* = 9.13 \times 10^{-29} m^3$.

In the range in which the temperature dependence of the flow stress becomes very small, i.e., in the lower temperature region of Fig. 11.14, the deformation is found to become quite inhomogeneous, with the deformation being almost entirely confined into a set of intense shear bands, as shown in Fig. 11.16. Here the tensile response of the samples becomes too unstable to perform strain rate change experiments. The specimens undergo early fracture inside the intense shear bands by the "meniscus instability" mechanism discussed in Section 11.3.3. In any case, however, the combination of negligible strain hardening and a decreasing strain rate sensitivity of the flow stress should result in hastened rupture by necking even if such fractures did not occur (Argon, 1973). In fact the mechanical instability is hastened further since the strong shear localization suggests the presence of a strain softening process. Much evidence (Megusar et al., 1982) indicates

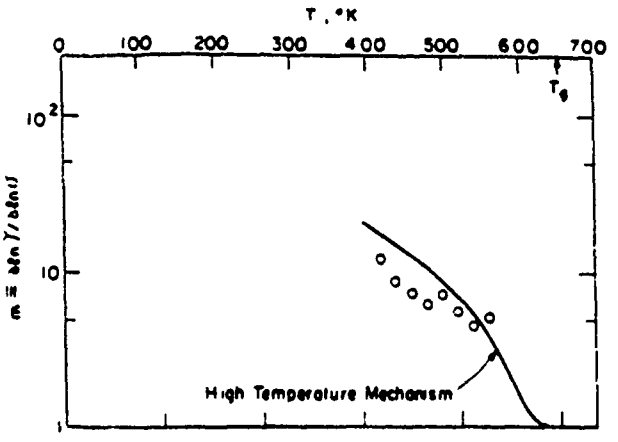

Figure 15: Figure 11.15: Temperature dependence of stress exponent of strain rate for a $Pd_{80}Si_{20}$ glass (Megusar, et al 1979).

that this strain softening is due to the strain induced generation of free volume which does not decay during deformation at low temperatures and high strain rates. The accumulating dilatation inside the sheared regions then results in a drop in plastic resistance which, in turn, rapidly concentrates the deformation further to form intense shear bands (Argon, 1979). Dilatometric measurements and associated kinematic analysis of shear localization in a $Pd_{77.5}$ Cu_6 $Si_{16.5}$ glass has verified that there are indeed very substantial density reductions inside shear bands which imply a flow dilatancy level of $\beta = d\theta/d\gamma$ of 0.018 and a total local retained dilatation of about 0.5 inside the bands for the total shear strains suffered by the bands of the order of 30 (Argon et al, 1985). Clearly, the level of inferred local dilatation can not have been uniformly dispersed but must have produced substantial cavitation. The reported tendency to form etch pits in shear bands (Pampillo and Chen, 1974) is most likely to be related to these supra-atomic scale cavities.

Figure 11.17 shows that there is a well-defined combination of strain rate and temperature which characterizes the bifurcation condition for formation of shear bands (Megusar et al., 1979). In the higher temperature and lower strain rate domain the strain induced free volume collapses diffusively as fast as it forms so that the plastic resistance remains relatively unaltered, and deformation remains homogeneous (Spaepen, 1977; Argon, 1979).

Operationally, the measurement of the plastic resistance of metallic glasses

Figure 16: Figure 11.16: Intense shear bands in a bent ribbon of a metallic glass Fe_{29} Ni_{19} P_{14} B_6 Si_2 (Argon, 1980).

in the lower temperature region is much more readily accomplished by means of indentation hardness measurements which circumvent most of the difficulties associated with mechanical instabilities in tension. Table 11.2 shows the Vickers micro-hardnesses of a collection of prominent metallic glasses obtained by Davis (1978). Applying the usual plastic constraint factor of 0.33 the tensile plastic resistances can be obtained from these measurements, and are also given in Table 11.2.

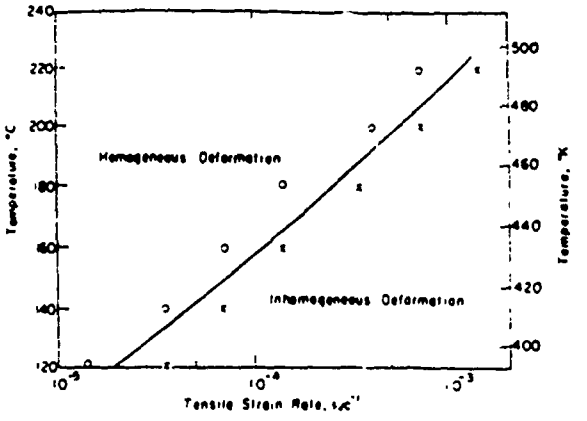

Figure 17: Figure 11.17: Regimes of homogeneous and inhomogeneous flow in a Pd_{80} Si_{20} glass (Megusar, et al, 1979).

Table 11.2 Young's Moduli E, Hardnesses H, and Plastic Resistances in Tension Y of a Selection of Metallic Glasses (Davis, 1978)

Alloy	E, (GPa)	H, (GPa)	$Y = (H/3)$, (GPa)
Pd_{80} Si_{20}	89.7	4.9	1.63
$Pd_{77.5}$ Cu_6 $Si_{16.5}$	89.7	5.0	1.67
Ni_{80} P_{20}	116.0	6.1	2.03
Ni_{40} Fe_{40} P_{14} B_6 (Metglass 2826)	127.0	7.5	2.50
$Fe_{80}P_{20}$	133	7.5	2.50
Fe_{80} B_{20}	169	11.0	3.67
Cu_{50} Zr_{50}	85.1	5.8	1.93
Cu_{50} Ti_{50}	98.6	6.1	2.03

11.4.1.4 Structural Aging and its Effects on Plastic Resistance

Since glass transitions resulting from higher cooling rates result in higher $T_g's$ and higher levels of frozen-in specific volume, structural compaction, or relaxation, can continue in the glassy state, if the temperature is not too low. Thus, the glass will undergo structural aging during which the density will systematically increase (as the free volume decreases), and all measurable mechanical properties will exhibit monotonic changes. Figures 11.9 and 11.12 show the resulting systematic decreases in internal friction and fluidity that accompanies structural aging in metallic glasses. The changes in hardness

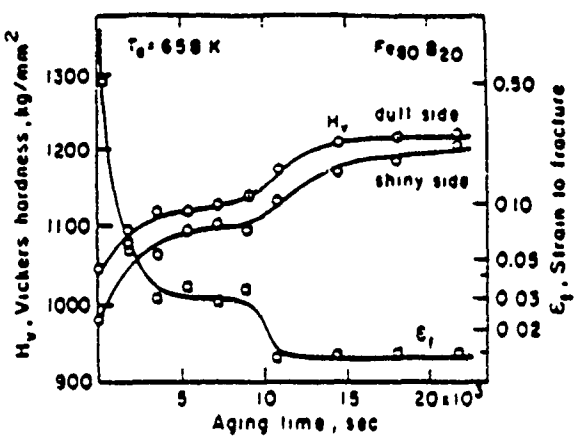

Figure 18: Figure 11.18: Changes in micro-hardness and strain to fracture of an Fe_{80} B_{20} glass as a function of aging time at 650 K (Deng and Argon, 1986a).

in a Fe_{80} B_{20} glass are shown in Fig. 11.18. Associated TEM studies have indicated that the rise in plastic resistance up to an aging time of 10^4 sec at a temperature of 0.96 T_g (0.92 of the crystallization temperature T_c) occurs as a result of structural aging in the glassy state alone without the benefit of crystallization. When crystallization sets in at times exceeding 10^4 sec a further rise is recorded in the hardness which results from the relatively high plastic resistances of the small crystallites that act as a first approximation as rigid filler in the amorphous phase (Argon, 1986). We note from Fig. 11.18 that the aging also results in a sharp reduction in strain to fracture, first in the amorphous range and then in the range where crystallization sets in where the crystallites evidently act as sites for cavitation.

Deng and Argon (1986b) have studied the kinetics of structural aging of metallic glasses and found evidence from a limited set of measurements that the distributed properties of structural aging resembles closely the distributed nature of shear relaxations under stress. As we will discuss in Section 11.4.3 below this, can be viewed either as a system with a distribution of relaxation times, obeying conventional Arrhernius kinetics or a process that obeys Williams-Watts kinetics characterized by so-called "stretched ex-

ponential" decays. (Deng et al., 1989c).

14.4.2 Model for Visco-Plastic Flow

Since access to the mechanism of visco-plastic flow in metallic glasses by direct experimental methods on the atomic level has not been possible, the results of various types of simulation of the process have provided considerable insight and guidance. One such fruitful simulation has been the amorphous Bragg soap bubble raft explored by Argon and Kuo (1979) and Argon and Shi (1982) which has indicated that based on this model the inelastic relaxations in atomic glasses is most likely to be by shear transformations, producing deformation in a manner sketched out in Fig. 11.8. In these experiments of simulating the plastic deformation in the sheared amorphous bubble rafts Argon and Kuo noted that the two dimensional forms of the sheared clusters could vary from concentrated forms of translation across nearly planar rows of bubbles to coupled diffuse rearrangements inside relatively equi-axed clusters, as depicted in Fig. 11.19.

The kinetics of inelastic straining by the diffuse shear mechanism, which is applicable in the low stress region of behavior could then be given readily for the 3-D variant, by a strain rate expression of the following form (Argon, 1979; Argon and Shi, 1982),

$$\dot{\gamma} = c\gamma^T \nu_G \exp(-\frac{\Delta F}{kT}) \sinh(\frac{\sigma\gamma^T \Omega c}{kT}) \tag{11.14}$$

where

$$\Delta F \approx (\frac{7-5\nu}{30(1-\nu)} + \frac{2(1+\nu)}{9(1-\nu)}\beta^2)\mu(\gamma^T)^2\Omega_e \tag{11.15}$$

is the Helmholtz free energy associated with a shear transformation occurring in a spherical region of volume Ω_e having a transformation shear strain γ^T and a transformation dilatation ϵ^T at the saddle point ($= \beta\gamma^T$) (Eshelby, 1957). In Eqns. (11.14) and (11.15), σ is the applied shear stress μ and ν are the shear modulus and Poisson's ratio respectively, while c is the volume fraction of the potentially transformable material and ν_G is the fundamental frequency of the clusters. This form of the visco-plastic strain rate would result in a phenomenological stress exponent of

$$m = \frac{\sigma\gamma^T\Omega_e}{kT} \cosh(\frac{\sigma\gamma^T\Omega_e}{kT}) \tag{11.16}$$

Comparing the predictions of the above model with the experimental measurements of Megusur et al (1979) and making use of the Bragg soap bubble raft simulations, the following values could be established: $\beta = 1.0; \gamma^T = 0.135; \Omega_c = 7.8 \times 10^{-28}$ in^3, for a Pd_{80} Si_{20} type metallic glass.

We note that when the applied stress decreases the non-linearity of behavior progressively decreases, the stress exponent $m \rightarrow 1$ and Eqn. (11.14) goes smoothly to an expression for Newtonian viscous flow and becomes

$$\dot{\gamma} = c(\gamma^T)^2 \nu_G (\frac{\sigma \Omega_c}{kT}) \exp(-\frac{\Delta F_v}{kT}), \tag{11.7}$$

where ΔF_v is now the activation energy of viscous flow and c may incorporate a structure given by Eqn. (11.12). The smooth change from linear to highly non-linear behavior as the stress is increased, and supporting the above picture was experimentally established by Taub (1980).

The strain rate expression that results for the concentrated shear process is given in turn (Argon, 1979) by

$$\dot{\gamma} = c\gamma^T \nu_G \exp(-\frac{\Delta G^*(\sigma)}{kT}) \tag{11.18}$$

where

$$\Delta G^*(\sigma) = 4.56 \hat{\tau} \Omega_c (1 - \frac{\sigma}{\hat{\tau}})^2; \quad \hat{\tau} = \hat{\tau}_{is} \tag{11.19a,b}$$

with $\hat{\tau}_{is}$ being the ideal shear strength of the structure, estimated to be 0.03 μ by comparison with results from 3-D computer simulations of Maeda and Takeuchi (1982).

The degree of agreement of the forms of the expressions given by Eqns. (11.14) and (11.8) when stated as flow stress relations, and compared with experimental results for Pd_{80} Si_{20} and $Pd_{77.5}$ Cu_6 $Si_{16.5}$ is shown in Fig. 11.14 and for stress exponent, is shown in Fig. 11.15. The agreement in the lower temperature region must be considered less good since deformation undergoes extensive shear localization where the smaller temperature dependence of the flow stress could be influenced strongly by the strain softening process referred to in Section 11.4.1.3 above.

11.4.3 Simulations of Plastic Flow in Metallic Glasses

Simulation of plastic shearing in the computer has been considered by many investigators as a fruitful avenue toward a better understanding of the kinematics of the process at the atomic level in a glassy metal. Of those,

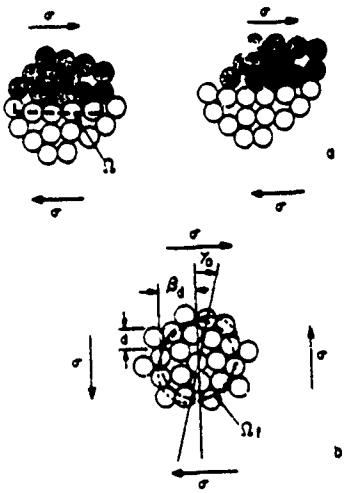

Figure 19: Figure 11.19: Idealization of two limiting forms of shear transformations observed in sheared soap bubble rafts: (a) concentrated shear translation, (b) diffuse shear transformation (Argon and Kuo, 1979).

the 3-D simulations of Maeda and Takeuchi (1982) and that of Srolovitz et al (1983) have pointed out the difficulties of required size of the simulation cell and those associated with extracting kinematical information out of 3-D space. To avoid these problems, of size and complexities in 3-D space, albeit at the risk of missing some degrees of freedom, Deng et al. (1989a) have chosen a relatively large 2-D simulation cell with periodic boundary conditions that had previously been melted and quenched in the computer. In this extensive simulation, as in nearly all others, individual atoms interact with each other by means of a Lennard-Jones potential, smoothly truncated between the third and fourth nearest neighbor atom. The details of the interatomic potential, and its application to 2-D simulations are given by Deng et al (1989a,d). Here we will discuss some of the more important findings of those investigators.

Figure 11.20(a) shows the starting configuration of atom environments after a perfect 2-D mat of hexagonal packing was melted and quenched in the computer to a temperature of $4 \times 10^{-3} T_m (5.56 \times 10^{-3} T_g)$ in a number of steps each incorporating some structural relaxation, followed by holding further at the final temperature. The resulting 2-D radial distribution function of the final structure, is shown in Fig. 11.20b. Several features of the mat in Fig. 11.20a must be noted. First, while the RDF shows the characteristics

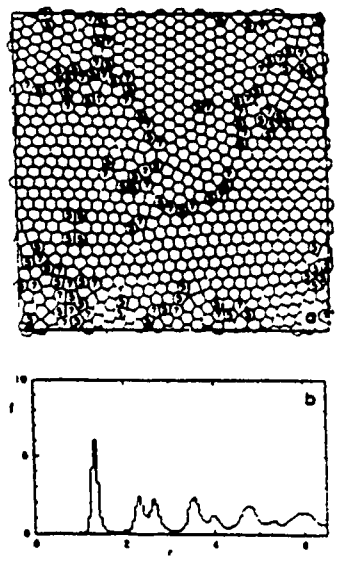

Figure 20: Figure 11.20 Arrangements of Voronoi polygons of atomic sites of a 2-D model glass quenched to $T/T_g = 4 \times 10^{-3}$. Note the 5-7 sided liquid-like material; (b) RDF of atom positions in (a). (Deng et al, 1989a).

of a well-relaxed glass, it is far from being homogeneously disordered. There is a substantial fraction of reasonably well-ordered material of hexagonal symmetry with characteristic dimensions of 8-10 atomic spacings. Second, the disordered material, readily recognizable by its chief ingredient of structural dipoles of atoms of 5 and 7 coordination makes up a volume fraction of 0.16 of the total. At the melting point this fraction is as high as 0.40 and percolates through the structure. The 5/7 coordinated structural dipolar material has an excess volume that is on the average 9% larger than a pair of hexagonal atom sites and can be viewed as a structural element of free-volume. Between T_m and T_g the 5/7 dipolar material fraction decreases monotonically to about 0.3, remaining, however, contiguous and maintaining the percolation condition. Below T_g the percolation condition is broken. In anticipation of the important properties of the 5/7 sided material resulting from its large free volume it has been identified as the liquid-like material of Cohen and Grest (1979).

The plastic deformation simulation has consisted of imposition of successive increments of external shear strain of 5×10^{-4} applied to the borders of the simulation mat, held at constant volume, followed by re-equilibration of the atoms by means of some structure relaxation to remove the most dis-equilibrium atom configurations. For each step of shear increment, after

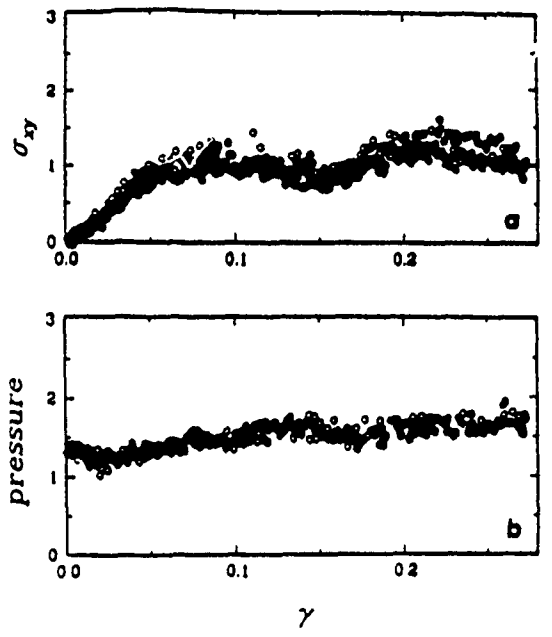

Figure 21: Figure 11.21: Shear response of 2-D model glass: (a) shear stress, shear strain curve; (b) increase of evoked pressure due to dilatancy effect (Deng, et al, 1989d).

re-equilibration was achieved, the atomic site stress tensor was calculated together with an atomic site strain increment tensor from the changes in the displacement gradients of each atom with respect to its immediate neighbors. Of particular interest were the two scalar invariants of the strain increment: the dilatation increment and the maximum (Mohr circle) shear strain increment. The process of shearing was continued in this manner until a total shear strain in excess of 0.27 was achieved for the simulation mat. Figure 11.21(a) shows the shear stress/shear strain curve for the mat.[1] A clear transition from nearly linear behavior to flow behavior occurs at a shear strain of about 0.05. Figure 11.21(b) shows that while the mat is plastically sheared at constant volume the external pressure on the mat increases slightly, but monotonically until a strain of 0.15 is reached, after which it remains constant. Figure 11.22 shows that when the shearing process is stopped at total strain levels of 0.025, 0.075 and 0.125 and is reversed, there is a prominent Bauschinger effect as reverse yielding is initiated even before complete unloading. The hysteresis is observed even in the apparent linear elastic range.

Examination of the distribution of deformations has resulted in the fol-

[1]The stresses in Fig. 11.21 are given in units of E_0/r_0^3, where E_0 is the binding energy of the pair potential, and r_0 is the separation between atoms where the pair potential goes to zero.

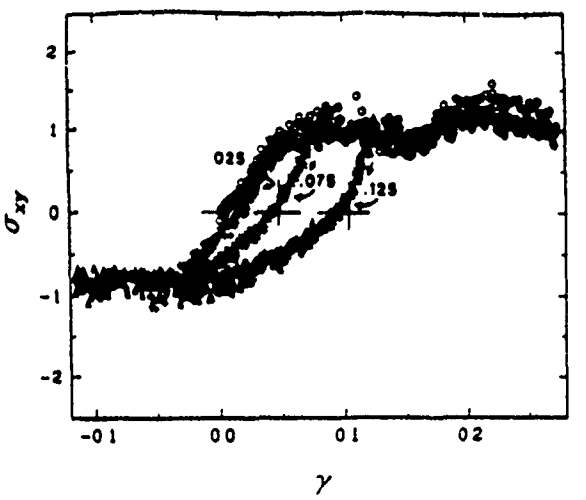

Figure 22: Figure 11.22: Simulation of reversal of shear in 2-D model glass showing pronounced Bauschinger effect (Deng, et al 1989d).

lowing findings:

a. Inelastic processes occur in the form of local shear transformations incorporating cooperative action of a number of neighboring atoms.

b. These transformations occur preferentially in regions where the liquid-like material (free-volume) congregates as is shown in Fig. 11.23 giving the distribution of local maximum shear strain increments at yield for a further step of external shear: (observe the resemblance of this distribution to the distribution of liquid-like material in Fig. 11.20(a)).

c. Inelastic processes, in the form of local shears in excess of the imposed affine shear, begin in the initial linear range (there is no real elastic limit).

d. The elastic-to-plastic transition occurs approximately when the total accumulated shear transformations become contiguous as was anticipated by Argon and Shi (1983) and as is familiar in crystal plasticity (Kocks, 1965).

e. At each stage of deformation, the residual back stresses of the shear transformations of the immediately preceeding history help reverse the deformation and are the cause of the large Bauschinger effect.

f. The shear transformations are generally dilatant (as observed to be the case by Argon and Shi (1982) in the soap bubble rafts) which results in the build-up of a system pressure when the deformation is performed at constant volume.

g. As a result of the deformation dilatancy the volume concentration of liquid-like material can fluctuate, this is shown in Fig. 11.24 where the variation of the liquid-like material concentration with strain is shown. Comparison of this with Fig. 11.21(a) shows that the depression in flow stress coincides with the peak in concentration of the liquid-like material.

h. Eventually when the deformation induced liquid-like material becomes contiguous, shear localization can set-in as is shown in Fig. 11.25 (a,b,c) as the total shear strain increases from 0.10-0.15-0.20. Prominent localization has occurred at a shear strain of 0.15.

i. At any stage of the deformation imposition of an external affine shear strain increment can evoke a substantial fraction of the local shears in directions other than the external shear increment – apparently relieving disorder related pre-existent misfit, and always reducing the Gibbs free energy of the entire system.

j. Finally, in all the observed sequences of deformation production of strain from motion of unambiguous crystal dislocations (displacement of isolated 5/7 dipoles) was quite rare resulting only in a fraction of about 0.11 of the total strain, but demonstrating the overwhelming efficiency of this mode of strain production when it is present.

Clearly, the results of the simulation that were presented relate to 2-D material which must quantitatively differ from what occurs in 3-D material. Nonetheless, the reported observations make up a complete set of phenomena which provide important insight not only into the deformation mechanism but also into the glassy state.

11.5 Inelastic Response in Space Network Glasses

Observation of anelastic and viscous behavior in space network glasses (oxide glasses) at elevated temperatures, but still under their T_g and at relatively small stresses, has been widely reported. (Jones, 1948; Argon,

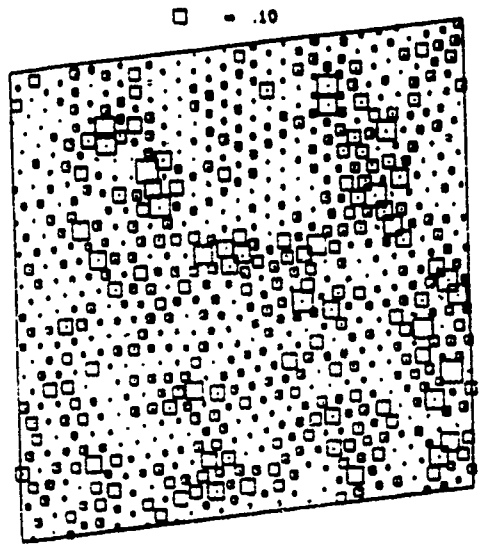

Figure 23: Figure 11.23: Distribution of atomic site maximum shear strain spikes in the sheared 2-D model glass (Deng et al 1989d).

1968). The distributed nature of relaxation times, in unmodified and modified network glasses measured by internal friction experiments or by creep and recovery creep experiments is very similar to that discussed in Sections 11.4.1.1 and 11.4.1.2 for metallic glasses (Argon, 1968).

Plasticity in network glasses, however, is quite unfamiliar, since they fracture under normal conditions in tension well before any non-linear behavior characteristic of plastic flow can be initiated. When fracture is suppressed, however, by the superposition of a large pressure or in micro-hardness experiments where a large pressure exists in the plastic flow field as an integral part, oxide glasses can undergo large strain plastic flow. The diverse, common and uncommon, experiments of many investigators carried out under such favorable conditions have been reviewed by Argon (1980). Of these the most informative are the micro-hardness indentation experiments of Marsh (1964a,b) on a soda glass and type E glass at different temperatures and indentation rates. These results are shown in Figs. 11.26(a) and (b), where the athermal intercept value of the plastic shear resistance $\hat{\tau}_0$ is the ideal shear strength which has been taken as $\mu/2\pi$ on a sinusoidal model of shear interaction of two parallel planes in the solid. The solid curves in these figures are the predictions of a variant of a homogeneous flow model similar to that discussed in Section 11.4.2 for metallic glasses. It parallels the results well

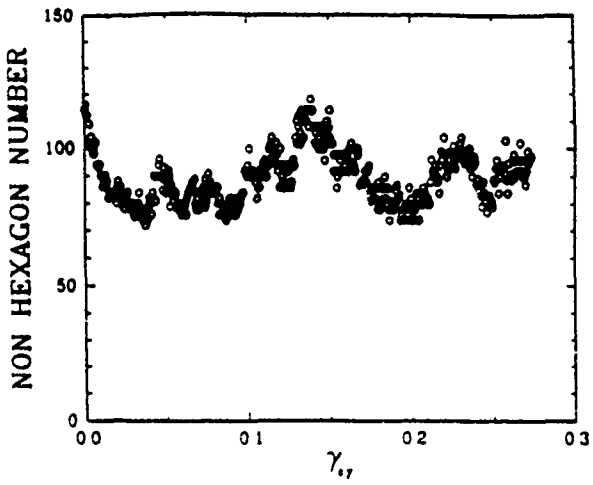

Figure 24: Figure 11.24: Variation with strain of the total number of liquid-like atomic sites in the sheared 2-D model glass (Deng et al 1989d).

in the low stress and high temperature region but severely underpredicts the plastic resistance at very low temperature or very high strain rate. This has been accounted for by Argon (1980) as a manifestation of a strong strength differential effect where the plastic resistance of a solid increases sharply with increasing pressure when the accompanying background mean normal elastic strains become very large. The dotted curves take such a strength differential into account based on the anticipated pressure dependence of the plastic resistance.

It is worthwhile to emphasize that plasticity of oxide glasses even under the most favorable conditions is very limited and of little technological importance. Thus, oxide network glasses can be considered as intrinsically brittle solids that will fracture before any significant plastic flow can occur under states of stress not containing a very high level of superimposed pressure component.

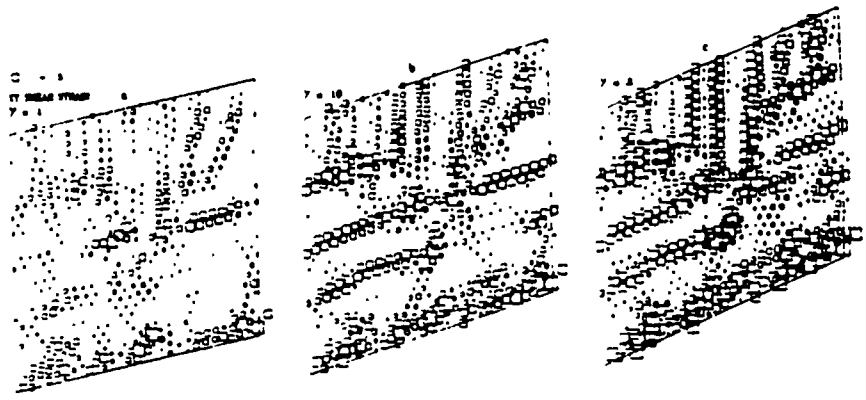

Figure 25: Figure 11.25: Sequence of development of shear localization in the sheared 2-D model glass: (a) after $\gamma = 10\%$; (b) after $\gamma = 15\%$ (c) after $\gamma = 20\%$ (Deng et al 1989d).

11.6 Inelastic Response in Polymeric Glasses

11.6.1 Experimental Observations

11.6.1.1 Anelasticity

The anelastic response of polymers has been studied extensively over a wide frequency range between $0K$ and the T_g (see McCrum et al, 1967). In these studies it has been customary to report not only the temperature dependence of the cyclic energy loss but also the so-called dynamic modulus as a function of temperature at a given frequency. As in the case of metallic glasses the spectral distribution of the mechanical relaxation times have been viewed as a sensitive probe of the structure of the polymer. Figure 11.27 shows the temperature dependence of the dynamic modulus and the associated internal friction ($\tan\delta$) spectrum of the atactic glassy polymer of polycarbonate of bisphenol-A(PC) which is typical of most such information for other polymers. Examination of Fig. 11.27, shows, however, that there are some discrete relaxations below the glass transition temperature which must have a specific molecular level interpretation. In PC, where the

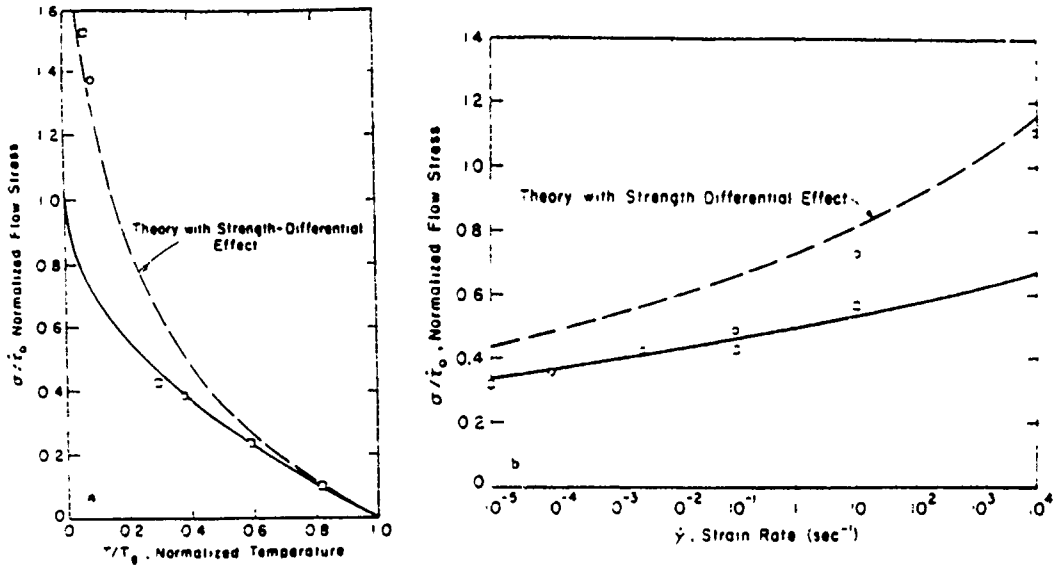

Figure 26: Figure 11.26: Temperature dependence (a) and strain rate dependence (b) of normalized flow stress of two network glasses: (□) E glass; (O) soda glass (Marsh, 1964a,b; Argon, 1980).

molecule contains a regular arrangement of phenylene rings, their rotation about the molecule axis can be a major component of a local shear relaxation. Similarly, other conformational rearrangements of specific molecular segments can also be responsible for these discrete relaxations superimposed on more diffuse rearrangements of the entire molecule. Such rearrangements have been discussed by McCrum et al (1967) and have also been partially simulated in the computer as we will discuss in Section 11.6.3.

11.6.1.2 Plastic Flow and its Mechanism

All glassy polymers exhibit plastic behavior under high stresses in compression where fracture can be suppressed in those that tend to be brittle in tension. In the subgroup of stiff chain thermoplastic glassy polymers which do not craze, or in which crazing can be suppressed, well developed plasticity is observed also in tension. A character feature of this plastic behavior, differentiating it from ductile metals, is the strong molecular orientation

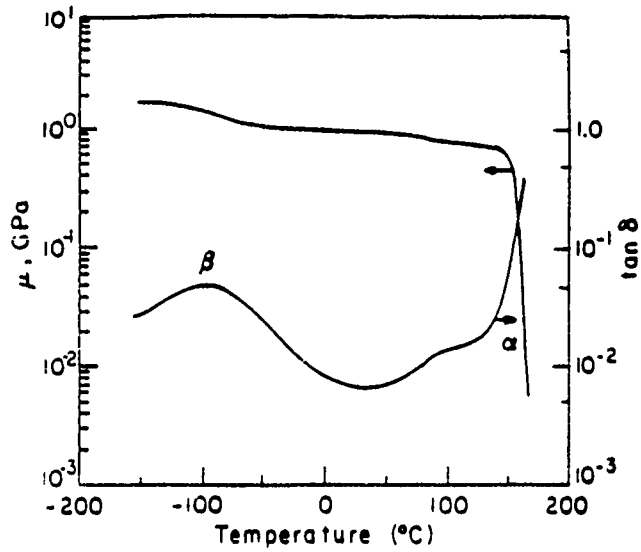

Figure 27: Figure 11.27: Temperature dependence of the shear modulus and cyclic energy loss in PC. (Kambour, private communication).

hardening that occurs at large strain which results in a sharp up-turn in the tensile plastic resistance curve, as is shown in the set of stress strain curves of PMMA in Fig. 11.28 (Hope, et al, 1980). The form of these curves is reminiscent of the large strain behavior of cross linked rubbers, albeit with a substantial additive component of strain-independent plastic resistance. That this resemblance is real is established from the nearly complete recoverability of shape of highly distorted glassy polymers when they are heated to above their T_g.

The temperature dependence of the yield strength of glassy polymers closely parallels the temperature dependence of the modulus as is shown in Figs. 11.29(a) and 11.29(b) for a set of stiff chain polyimides (Argon and Bessonov, 1977a). This indicates that the plastic resistance is governed primarily by intermolecular interactions. The dependence of the inelastic strain rate on the applied stress is a strongly non-linear one, also reminiscent of metal plasticity, as the results for polyethylene-terephthalate (PET) in Fig. 11.30 show. Argon and Bessonov (1977a) have carried out experiments on the strain rate dependence of the tensile or compressive yield strength of a series of glassy polymers ranging from flexible chain polymers to some stiff chain polymers to probe the shear activation volumes Δv^* of the plastic flow

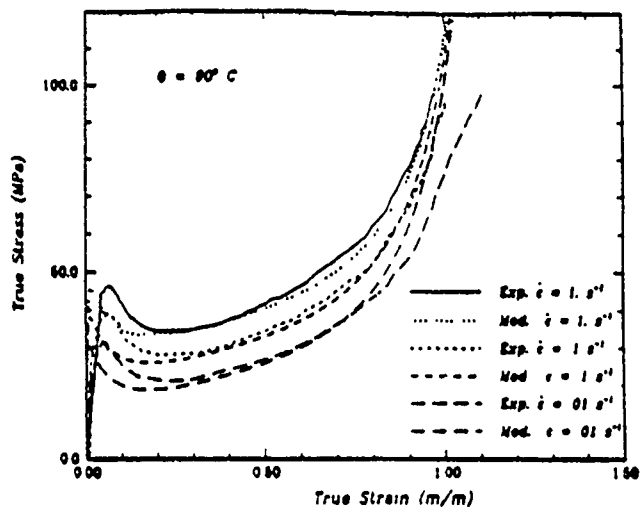

Figure 28: Figure 11.28: Tensile true stress, true strain curves for PMMA at 90C (Hope et al 1980; Boyce et al 1988a).

event. Their results are given in Table 11.3.

Table 11.3 Shear Activation Volumes Δv^*, and Actual Volumes Ω_c of Relaxing Clusters of Glassy Polymers

Polymer	$\Delta v^*, (m^3)^\dagger$	$\Omega_f (m^3)^\ddagger$
PS	284×10^{-30}	0.78×10^{-26}
PMMA	375	1.01
PET	991	2.68
PC	1060	2.86
PPO	613	1.66
R-R	1030	2.78
DFO	1710	4.62
Kapton	2280	6.16

† From experiments of Argon and Bessonov (1977a).
‡ Calculated using $\gamma^T = 0.037$ based on simulation of Mott et al (1991).

Calorimetric experiments of Oleynik (1990) and co-workers (Rudnev, et al, 1990) have revealed important and striking parallels of the plasticity of glassy polymers to that of glassy metals discussed in Sections 11.4.1-11.4.3.

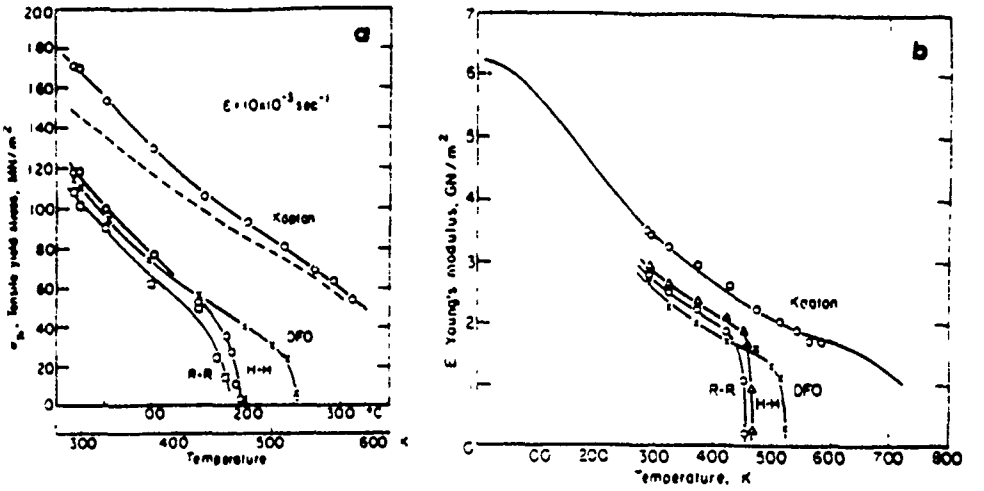

Figure 29: Figure 11.29: Temperature dependence of tensile yield stress (a); and Young's modulus (b); of a set of polyimides; (R-R) resorcinol; (H-H) hydroquinone; (DFO) oxydiphenyl (Kapton) pyro-melitic acid (Argon and Bessonov, 1977a).

Their coordinated measurements of stress strain behavior, concurrent deformation calorimetry (DC) and subsequent differential scanning calorimetry (DSC) have established that heat evolution begins below yield and monotonically and smoothly increases with increasing strain to a relatively high rate $\dot{Q}$, paralleling the overall plastic work rate $\dot{W}$ at a strain of about 25%, as is shown for the case of atactic polystyrene (a-PS) in Fig. 11.31. At that stage the stored energy of cold work, ΔF, reaches a steady state (presumably dependent, to some extent on the applied strain rate), while there are still no important changes in infra-red (IR) spectroscopy indicating that significant, large scale changes in molecular conformations have not occurred. The DSC measurements have shown that on samples deformed to plastic strain (compression) levels of 10-30%, cooled under stress to low temperatures, followed by stress removal, and upon heating, stored energy release begins at the previous deformation temperature, and has a characteristic bi-modal spectrum shown in Fig. 11.32 for an epoxy-aromatic amine network (EAN) polymer. The sharp high temperature peak occurring at T_g (= 140 C) is related to conformational recovery, while the broad low temperature hump, starting from the previous deformation temperature is of a different, non-conformational, character, and is more akin to the stored elastic strain energies around shear transformations discussed in Section 11.4.2 for metallic glasses. Moreover,

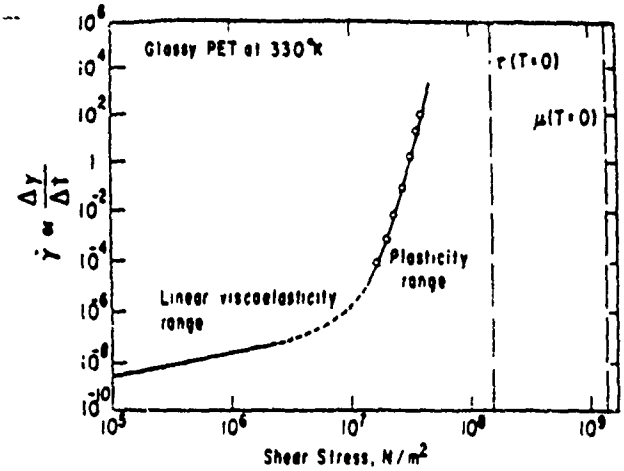

Figure 30: Figure 11.30: Stress dependence of the inelastic strain rate in PET at 330K. At the mechanical threshold stress the strain rate becomes unbounded (Argon and Bessonov, 1977b).

these investigators have established that in lightly strained samples only the low energy hump is present, and that the appearance of the conformational peak requires strains in excess of those where ΔF reaches its initial plateau value. This indicates that the development of the molecular orientation, characteristic of large strain behavior akin to cross linked rubbers, requires the establishment of a steady plastic flow state. The validity of the above sequence of processes is verified by the results of computer simulations of plastic flow in vinyl polymers that we will discuss in Section 11.6.3.

11.6.1.3 Kinetics of Plastic Flow

While the actual kinematics of molecular segment rearrangements during the plastic deformation of glassy polymers remains elusive, mechanism inspired and quite successful constitutive laws can be stated for deformation in the glassy state. One such formalism is that of Argon (1973). In this approach a specific form of strain producing molecular segment rotation is conceived and the saddle point free energy ΔG^* for it is calculated in terms of some molecular scale parameters. The resulting Arrhenius rate expression for plastic shear strain rate is

$$\dot{\gamma} = \dot{\gamma}_G \exp(-\frac{\Delta G^*}{kT}) \qquad (11.20)$$

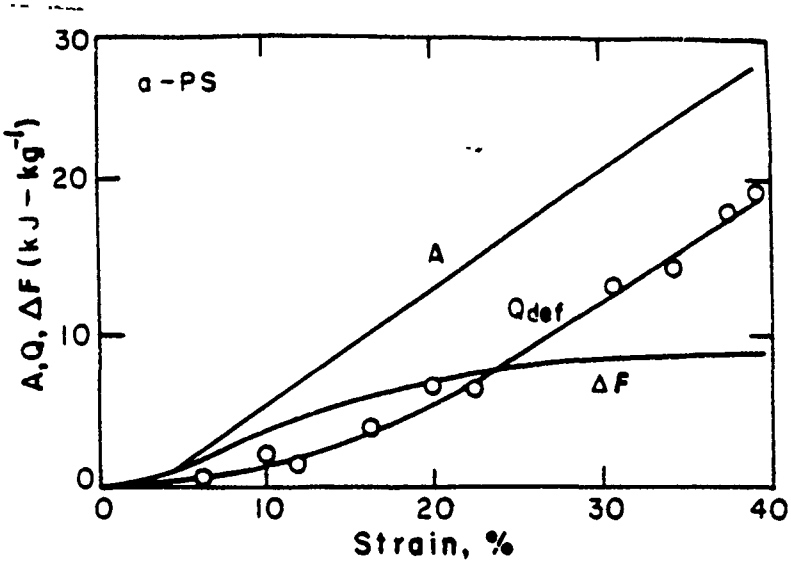

Figure 31: Figure 11.31: Rate of mechanical work expenditure, ($\dot{A}$); free energy storage (ΔF); and evolution of heat ($\dot{Q}$) during the plastic deformation of atactic PS (Oleynik, 1990).

with

$$\Delta G = \Delta G_0 (1 - (\frac{\sigma}{\hat{\tau}})^{\frac{5}{6}}) \qquad (11.21a)$$

$$\Delta G_0 = \frac{3\pi\mu\omega^2 a^3}{16(1-\nu)} \quad \therefore \hat{\tau} = 0.077\mu \qquad (11.21b,c)$$

Argon and Bessonov (1977a) have noted that this constitutive form can be stated as

$$(\frac{\sigma}{\mu})^{\frac{5}{6}} = A - B(T/\mu). \qquad (11.22)$$

where

$$A = (\frac{0.077}{(1-\nu)})^{\frac{5}{6}} \quad \therefore \quad B = A\frac{16(1-\nu)k}{3\pi\omega^2 a^3} ln(\dot{\gamma}_G/\dot{\gamma}) \qquad (11.23a,b)$$

are material constants. That this is indeed the correct form of the constitutive behavior for the thermoplastic glassy polymers listed in Table 11.3 is shown in Figs. 11.33(a) and 11.33(b) and for a DGEBA (di-glycidyl ether of bisphenol-A) epoxy thermoset polymer in Fig. 11.33(c) (Yamini and Young,

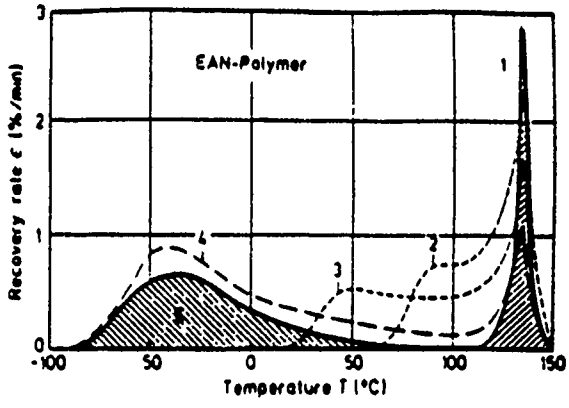

Figure 32: Figure 11.32: Strain recovery spectrum with temperature of previously deformed EAN-polymers: (1) $T = 150C$, $\epsilon = 0.04$; (2) $T = 60C$, $\epsilon = 0.11$; (3) $T = 20C$, $\epsilon = 0.09$; (4) $T = -85$ C, $\epsilon = 0.12$; $T = -85C$, $\epsilon = 0.045$ (Oleynik, 1990).

1980). More extensive discussions about the possible molecular level meanings of the above form of the constitutive relation were provided in the original reference.

When large strains are suffered by the glassy polymer, strain induced molecular orientation produces an important back stress to deformation that can be modeled as a first approximation by the entropic resistance of rubber elasticity (Haward and Thackray, 1968; Argon, 1973; Boyce et al, 1988a) which gives the following principal back stress (resistances);

$$B_i = \rho \frac{RT}{3M_e} \lambda_i \{ \lambda_i \mathcal{L}^{-1}(\lambda_i/\lambda_n) - \frac{1}{3} \sum_{j=1}^{3} \lambda_j \mathcal{L}^{-1}(\lambda_j/\lambda_n) \} \tag{11.24}$$

where $\rho RT/M_e$ is the rubbery regime shear modulus, λ_i are the principal extension ratios, λ_n the uniaxial locking stretch of the polymer where full molecular orientation occurs, and $\mathcal{L}^{-1}$ is the inverse Langevin function (Boyce et al, 1988a). Figure 11.28 shows the agreement between experimental results and the theoretical formalisms represented by Eqns. (11.20-11.24). This constitutive relation for the plastic resistance incorporating other improvements related to strain softening, aging, and pressure dependence of the plastic resistance has been used extensively by Boyce et al (1988a,b; 1989) in computational applications of boundary value problems for large strain deformation processing.

The above theoretical model is meant to apply for deformation in a stable

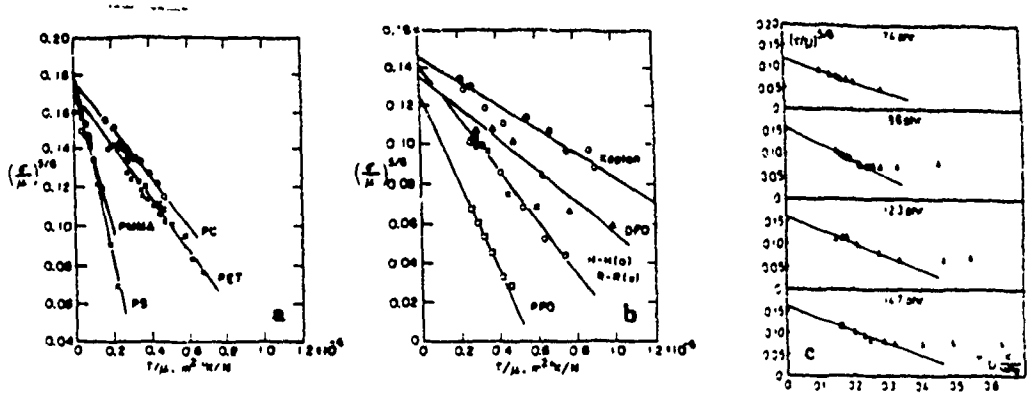

Figure 33: Figure 11.33: Dependence of normalized plastic shear resistance on temperature for a series of glassy polymers. The straight lines fit the form of the model of Section 11.6.1.3 (a) Flexible chain polymers; (b) stiff chain polymers (Argon and Bessonov, 1977a); (c) DGEBA - epoxy polymer (Yamini and Young, 1980).

structure where an increase in temperature only accelerates the kinetics of transfer of deformation units from unflexed to flexed. Near a glass transition where a temperature increase produces important structural alterations that increase the fraction of liquid-like material (see Section 11.4.3), different considerations are necessary to change the emphasis from inter-molecular to intra-molecular resistances to deformation. This was achieved by Robertson (1966, 1968) in a theoretical model in which thermal equilibrium concentrations of strain producing "flexed" molecular conformation under the applied shear stress are calculated from Boltzmann statistics through which a structural reference temperature θ (above T_g) is defined that in turn defines the effective deformation resistance through the free volume model of the glass transition of Williams, Landel and Ferry (1955). Argon and Bessonov (1977a) have compared the Robertson model to theirs and have concluded that it should be the model of choice near T_g.

11.6.2 Dilatational Plasticity in Glassy Polymers

As discussed in Section 11.3.2.2 certain glassy polymers undergo crazing in tension leading to a mode of dilatational plasticity. While the molecular level requirements for a crazing vs non-crazing response are not well estab-

lished, two complementary conditions are known to be important. First, polymers that undergo crazing are predominantly flexible chain material which are known to have unusually high atomic level stresses due to a high degree of molecular structural disorder. (Theodorou and Suter 1986a,b), while non-crazable polymers tend to be stiff chain material with considerable evidence for short range order – and possibly having much lower atomic level disorder stresses (Argon and Cohen, 1990). Second, non crazable polymers include those that have very high levels of entanglement densities, resulting in very small natural draw ratios, not permitting the formation of craze matter fibrils (Kramer, 1983).

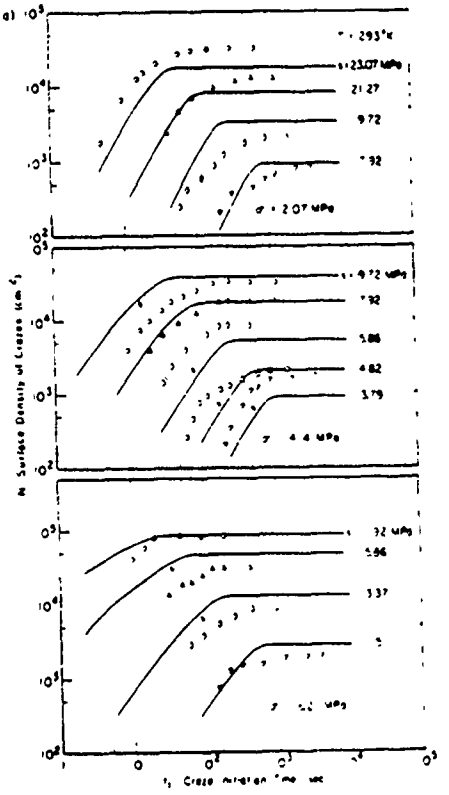

Figure 34: Figure 11.34: Dependence of craze initiation time on different levels of negative pressure and deviatoric shear stress at room temperature in atactic PS (Argon and Hannoosh, 1977).

Initiation of crazes is a rate process that is sensitive to a certain combination of the deviatoric shear component s, and the negative pressure σ_m of the local applied stress. Figure 11.34 shows a set of experimental observations of

Argon and Hannosh (1977) on craze initiation time t_i, from the surfaces of polystyrene (PS) samples with a known level of controlled micro-roughness, subjected to different combinations of s and σ_m. This combination can be stated as a craze initiation rate as follows:

$$\text{Rate} = \frac{1}{t_i} = C_1 \exp\left(\frac{3\sigma_m}{2QY} - \frac{C_2}{s}\right). \tag{11.25}$$

The constants C_1, C_2, Q ($C_1 = 166 \times 10^7 \text{sec}^{-1}; C_2 = 0.95\text{GPa}; Q = 0.0133$ at 295 K (Piorkowska, et al, 1990)) are material parameters with the above experimentally determined values being appropriate for PS at room temperature; and where Y is the tensile plastic resistance. A mechanistic rationale for the above form has been given by Argon and Hannosh (1977).

Crazes viewed as dilatational transformations, as discussed in Section 11.3.2.2, grow by the continued conversion of solid polymer into spongy or fibrillar craze matter by displacing the craze borders under a tensile stress acting across the craze plane. This conversion has been established to be by an interface convolution process (Argon and Salama, 1977; Kramer, 1983) that results in the following overall craze strain rate,

$$\dot{\epsilon}_c = \epsilon^T \frac{d}{dt}(Ah) \tag{11.26}$$

where A is the total craze area per unit volume, and h is the primordial craze thickness undergoing the tensile transformation strain ϵ^T. In the early stages of crazing the craze thickness tends to remain fixed, and

$$\dot{\epsilon} \rightarrow \epsilon^T h \rho v_{ct} \tag{11.26a}$$

where ρ is the active craze front length per unit volume and v_{ct} is the craze tip velocity, transverse to the applied tensile stress. In the latter stages of crazing when the total craze area per unit volume remains relatively fixed and the craze widens by translating the craze borders, the craze strain rate becomes

$$\dot{\epsilon}_c \rightarrow \frac{2\epsilon^T}{1+\epsilon^T} A v_{cb} \tag{11.26b}$$

where v_{cb} is the craze border velocity, in the direction of the applied tensile stress σ and the factor 2 arises from the fact that the craze can thicken by the outward displacement of both of its borders. The craze front velocity and the craze border velocities have a kinetical dependence on the applied stress σ given by (Argon and Salama, 1977; Piorkowska, et al, 1990)

$$v_{cb} = \alpha v_{ct} = \alpha v_o \frac{\hat{Y}}{\sigma} \exp\{-\frac{\Delta G_0}{kT}[1 - (\lambda'_n \frac{\sigma}{\hat{Y}})^{\frac{1}{6}}]\}. \qquad (11.27)$$

In Eqn (11.27) $\hat{Y}(= 0.133\mu/(1-\nu))$ is the athermal plastic resistance of the glassy polymer, λ'_n is an orientation hardening-modified extension ratio of the craze matter v_o is a pre-exponential rate constant, α a geometrical constant and ΔG_0 is an effective activation free energy of plastic flow (Eqn. 11.2b). For PS at room temperature ($\alpha = 0.282; v_0 = 1.23 \times 10^6$ m/sec; $\Delta G_0/kT = 44.7; \lambda'_n = 1.85$; (Piorkowska, et al, 1990)).

For additional details of craze plasticity, the effect of polymer type, molecular weight, and related matter, the reader is referred to the two treatises edited by Kausch (1983, 1990). Finally, it should be noted that while crazes do transform the continuous polymer to a discontinuous spongy form it can nevertheless, result in very substantial overall strains – provided that the crazing process is carefully "managed" to occur at stress levels that do not result in craze fracture (Volynskii and Bakeev, 1984).

11.6.3 Simulation of Plastic Flow in Glassy Polymers

11.6.3.1 Molecular Structure Models

As in the case of atomic glasses discussed in Section 11.4.3, in polymeric glasses the molecular level process of plastic deformation can be very effectively simulated by computer.

Considering the interactions between atoms along the back-bone of a chain molecule of a polymer glass, it is found that relative separation of atoms as well as flexing of bound angles between atoms along the molecule are very strongly resisted. In comparison, the rotation of molecular groups about a bond needs to overcome only a modest torsional restoring moment which tends to make chain molecules conform primarily by rotation along the back-bone bonds. Thus, as a first approximation the back-bone bonds act as inextensional and bond angles as inflexible. In addition, in a dense arrangement of chain molecules, portions of the molecule will interact with portions of surrounding molecules by van der Waals interaction. Based on these idealizations, utilizing known forms of torsional potentials and van der Waals interactions molecular structures of several glassy polymers have been obtained by static energy minimization techniques. These include polypropylene (PP) (Theodorou and Suter, (1985, 1986a,b) polyvinyl chloride (PVC)

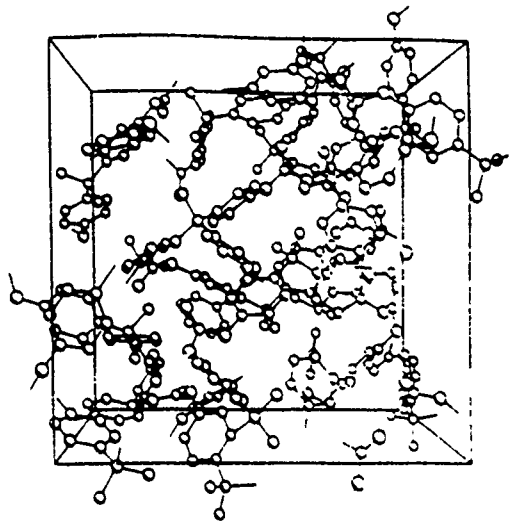

Figure 35: Figure 11.35: The molecular structure of a typical configuration of glassy PC of bisphenol-A (Hutnik, et al 1991a)

(Ludovice and Suter, 1991), polycarbonate of bisphenol-A (PC) (Hutnik et al, 1991a). Figure 11.35 shows a typical fully dense configuration of glassy PC in the form of a single molecule of molecular weight of 4.53 kg/mole together with its many images reflected back into, and filling a cube with periodic boundary conditions. The atomic radii in this figure have been reduced in size to permit viewing into the structure. The details of how these molecular structures are obtained from the best information on interatomic force fields are too extensive to be presented here. The interested reader must consult the above references for this detail. It should suffice here to state that these structures that have been obtained for the appropriate densities, have x-ray scattering factors, cohesive energy densities, and elastic properties that agree very well with corresponding experimental results. They all have rather high atomic level stresses that have root mean square values of the same order as the elastic moduli themselves, and are thus about a factor of 3 higher than the corresponding stresses in atomic glasses on a normalized basis. Below we will discuss simulations of molecular segment relaxations in PC that play a role in internal friction and large strain pure shear deformation in PP.

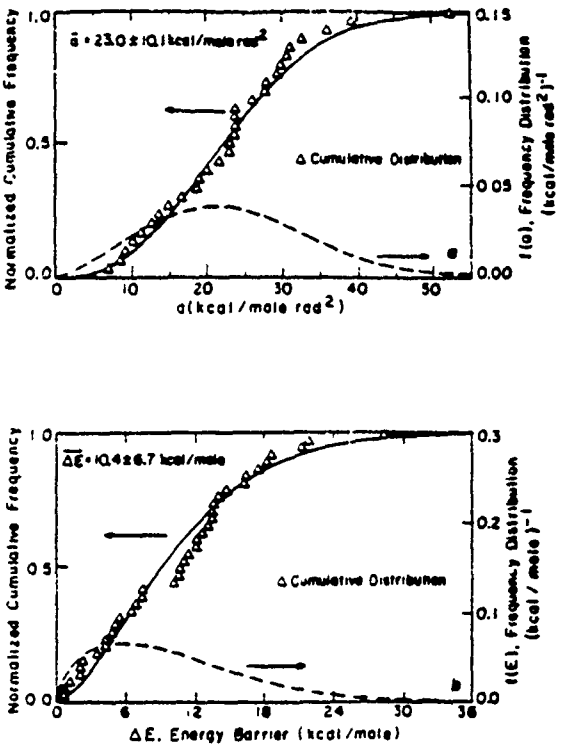

Figure 36: Figure 11.36: Energetic characteristics of phenyl ring rotations in PC: (a) cumulative distribution and frequency distribution of curvatures of energy wells of rings; (b) distribution of peak energy barriers to ring rotations (Hutnik et al 1991b).

11.6.3.2 Segment Relaxations in PC:

The so-called β relaxation, loss peak shown in Fig. 11.27 in PC has commonly been attributed to a local shear relaxation process involving, at least in part, the rotation of a phenyl ring, or alternatively involving a conformational rearrangement in another specific atomic group along the chain backbone such as perhaps the carbonate group. These possibilities were investigated by Hutnik et al (1991b) in molecular structure models such as the one shown in Fig. 11.35, by imposing increments of rotation to a selection of phenyl rings, fixing the rotation angle in one or the other bonds on either side of the ring, followed by energy re-minimization of the entire structure. This

has resulted in either the actual rotation of the ring or, in some cases, in the conformational rearrangement in the adjoining carbonate group. For either case the derived potential contour along the reaction path for the imposed change exhibited clear energy maxima, bounding ranges of stable flexing of the local system. Figures 11.36(a) and 11.36(b) show the cumulative distribution and frequency distributions of the curvature a of the local energy well and the peak energy barriers ΔE respectively for the phenyl ring rotations. Considering the ring in its potential well as a rotational simple harmonic oscillator, its frequency factor ν_G can be obtained as

$$\nu_G = \frac{1}{2\pi}\sqrt{\frac{2\bar{a}}{J}} \tag{11.28}$$

giving an overall rotational transition rate R (reciprocal average waiting time for ring rotation)

$$R = \nu_G \exp(-\frac{\Delta E}{Rt}) \tag{11.29}$$

where J is the effective rotational mass moment of inertia of the phenyl ring. Using appropriate values for the latter and the average value of $\bar{a} = 23$ kcal/mole rad^2, $\nu_G = 2.3 \times 10^{12}$ Hz was found. The average value $\overline{\Delta E} = 10.4 \pm 6.7$ kcal/mole for the energy barrier for ring rotation obtained from the simulation compares very well with the range of experimental values from 9.1 to 12.0 kcal/mole measured in NMR experiments. The distribution of energies given in Fig. 11.36(b) is extremely broad ranging up to nearly 30 kcal/mole in comparison. The intra-molecular energy barrier for a ring rotation in an isolated molecule in solution is, in comparison, only in the neighborhood of 3 kcal/mole. Thus, clearly the energy barrier to ring rotation is primarily of an intermolecular nature. That this is so has been verified by noting that the segmental displacements in the surroundings of a rotating ring are always far reaching.

A complementary simulation of the conformational rearrangements of the carbonate group have given an equally broad distribution of energies with an average of $\overline{\Delta E} = 10.1 \pm 6.5$ kcal/mole.

These barrier energies for ring rotation and carbonate group rearrangements are considerably higher than the experimental value of about 7 kcal/mole. Clearly, when stimulated by external conditions of imposed cyclic strains the material will respond by selecting the lower energy portion of available processes. There is initial evidence from additonal simulations of large strain plastic behavior that local shear relaxations in PC have indeed important components of recognizable ring rotations. Considering that the simulations

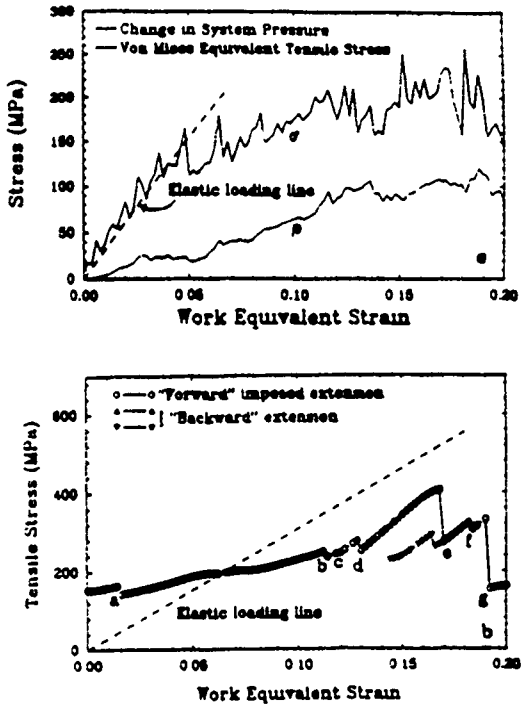

Figure 37: Figure 11.37: Simulation of stress-strain relation in the plastic deformation of atactic PP at 253K: (a) stress-strain curve for an average of 9 configurations; the lower curve shows the increase of system pressure under constant volume due to the dilatant nature of the deformation; (b) stress-strain curve for a single configuration (Mott et al, 1991).

with their imposed rotations, must be an upper bound, the agreement between them and anelastic damping experiments is encouraging.

11.6.3.3 Large Strain Plastic Shear of PP

A molecular structure model of glassy PP of a molecular weight of 2.968 kg/ mole (= 76 monomer units) similar to that shown in Fig. 11.35 for PC, and having a density and thermal properties appropriate for a temperature of 233K ($= T_g - 20$) was subjected to increments of extension of 2×10^{-3} along one edge of the cube and -2×10^{-3} along one of the transverse directions, to achieve conditions of pure shear at constant volume (Mott et al, 1991). In the fully equilibrated structure, after each increment of deformation, the atomic site stress tensors and strain increment tensors were calculated for

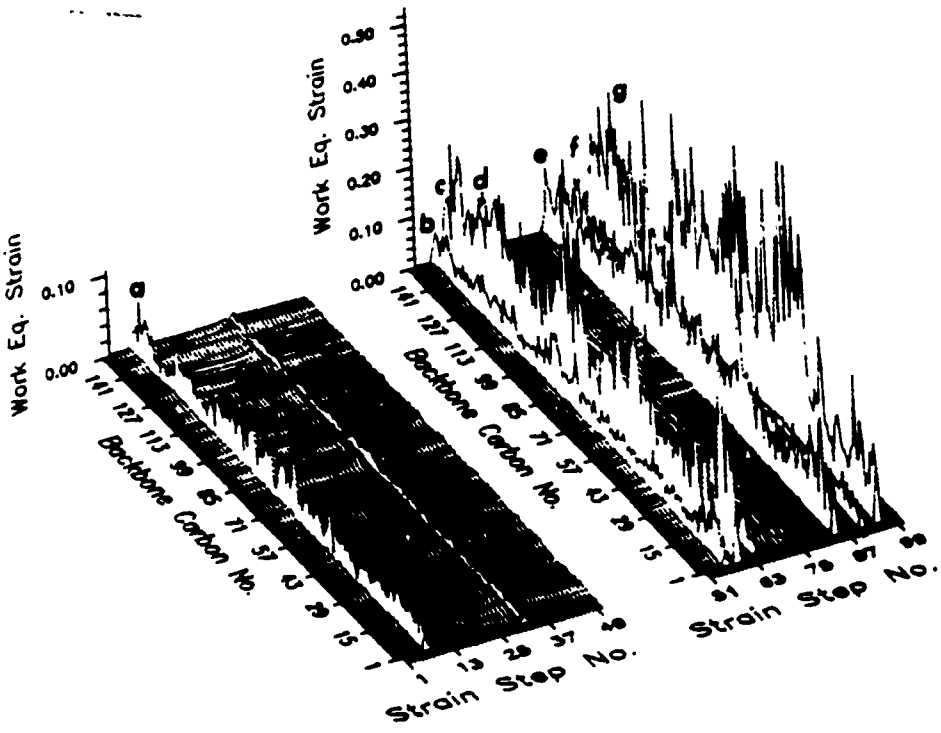

Figure 38: Figure 11.38: The chronology of the development of plastic strain increments for each backbone carbon atom on the PP molecule for the stress strain response of Fig. 11.37(b). The extensive "plastic" activity along the entire length of the molecule coincides with the sharp stress drops a-g shown in the figure (Mott, et al, 1991).

each atom. Figure 11.37(a) shows the resulting deviatoric tensile stress-strain curve obtained from the volume average stress and strain increments for a configuration average of 9 such simulation experiments. Figure 11.37(b) shows the tensile deviatoric stress-strain curve of just one of these configurations. The latter curve which samples the behavior of only a very small volume element has a high initial atomic level "stress noise" which is much reduced in Fig. 11.37(a) in the configuration average of 9 such responses. The configuration average behavior of Fig. 11.37(a) shows clear yielding behavior at a strain of about 5%, a broad transition to fully developed flow at about 10% and no important hardening after this. It also shows that the system pressure increases monotonically, up to about 10%, strain due to the fact that the deformation of the glassy material is of a dilatant nature and was enforced at constant volume. While more "noisy", the response of the single configuration shown in Fig. 11.37(b) shows important detail. It shows no clear elastic to plastic transition in the early stages but rather a

protracted reversible anelastic behavior to about 10%. After this range of straining, which has apparently mechanically polarized all pockets of more compliant material, the behavior becomes a succession of reversible elastic loading steps, with the expected slope, followed by abrupt and discrete steps of large irreversible plastic relaxations occurring at constant overall strain. Figure 11.38 shows a "spike map" of deviatoric atomic strain increments for each of the 153 back-bone carbon atom sites for each of the 100 strain increment steps. Clearly, outside the seven large plastic drops where intense strain activity is registered at nearly all atom sites, the strain increments during the other intervening 93 imposed strain steps are very small and at a background level. Intensive examination of molecular segment motions in the large plastic drops, by several techniques, including incremental stereo-imaging, revealed no readily recognizable recurring segmental motions, but established that the relaxations are far reaching, over the entire simulation cell having a volume of 60×10^{-27} m^3. Simulations carried out on a volume of $4.7 \cdot 10^{-26}$ m^3 gave similar but far less noisy results, suggesting that the inextensional bonds and inflexible bond angles of the molecules can accommodate the transformation shear strains of the plastic events by complex cooperative rotations about bonds only over substantially large volume elements. To verify this, first the distribution of transformation shear strains γ^T was computed from the plastic stress drops and is shown in Fig. 11.39. The average value of this broad distribution is $\gamma^T = 0.037 \pm 0.035$. Then, the calculated transformation shear strain distribution of the plastic stress drops of the simulation was compared with the experimentally determined activation volumes of Tables 11.3. Recognizing that the measured activation volumes are products of the transformation shear strain γ^T and the actual volumes Ω_e of the regions undergoing the relaxation, estimates of these volumes were obtained for all the polymers in Table 11.3 on the assumption that the average values of γ^T are of similar magnitudes as those given in Fig. 11.39 for *PP*. These computed volumes Ω_e are given in the last column of Table 11.3, and indicate that the plastic relaxations indeed require cooperative segmental rearrangements over a large volume.

The pure shear simulation has also searched for the rate of development of orientational alignment of segments over the range of straining of up to 20% axial extension. No significant development of molecular orientation above the background "noise" level was found. From all of these it must be concluded that the early regions of plastic deformation in glassy polymers bear a remarkable similarity to deformation in atomic glasses. Both undergo deformation by localized, elastic strain-energy-storing shear transformations which, however, are less localized in glassy polymers because of the con-

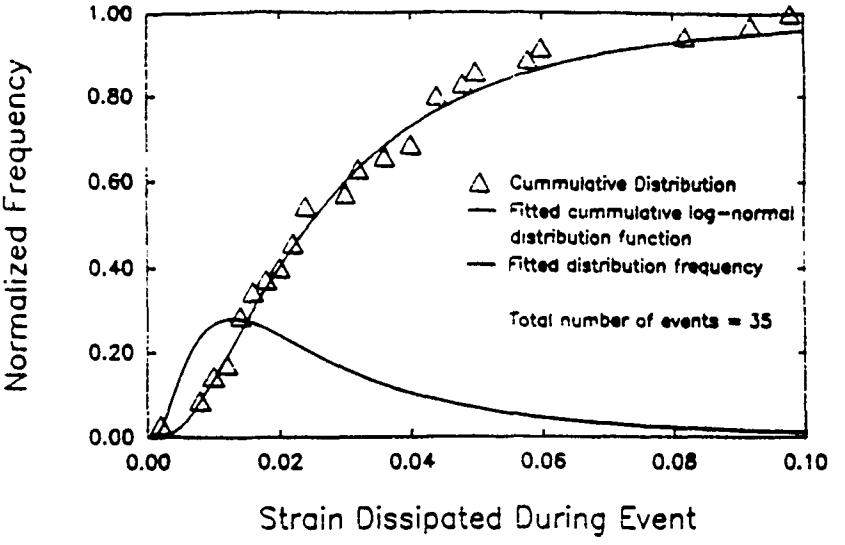

Figure 39: Figure 11.39: Distribution of "transformation" shear strains calculated from the discrete stress drops in the 9 separate configurations entering into the stress-strain response of Fig. 11.37(a). The figure shows both the cumulative distribution and the frequency distribution (Mott, et al, 1991).

straints imposed by the chain molecule. Recognizable free energy storage by reduction in configurational entropy that must eventually occur to account for the complete recoverability of shape change above T_g apparently does not set-in until the later stages of deformation, all in very good agreement with the deformation calorimetric measurements and post deformation DSC measurements of Oleynik (1990).

In a partial simulation of molecular motions in a glassy polymer undergoing tensile extension, Yannas and Luise (1983) have obtained estimates of the deformation resistance using interatomic pair potentials, based on an assumed uncoiling motion of molecules which they have labelled "Strophon" motion. The above simulations indicate that this view has considerable

merit.

11.7 Fracture of Glasses

11.7.1 The Fracture Instability

The role of cracks and flaws in brittle fracture under monotonic loading has been well appreciated since the pioneering work of Griffith (1920, 1924). The modifications that are necessary to Griffith's theory to understand fracture in more or less plastically deformable solids have been subjects of intense interest to ever-widening groups of researchers. The basic directions to these developments were given early by Orowan (1949) and by Irwin (1948), who in particular founded the branch of study of fracture mechanics that concerns itself with the precise statement of the condition of the fracture instability in structural components. Discussion of this very extensive subject will be outside the scope of this chapter. We shall find it sufficient to note that, for relatively low levels, of inelastic deformation that is necessary to propagate a crack in a solid, the condition of the fracture instability can be stated alternatively: as a critical stress intensity factor K_I; a critical crack opening displacement δ_{co} defined at the root of the crack; or a critical energy release rate G_I. These terms, defined for tension in relation to the macroscopic parameters under the control of the experimenter, are given for a plane strain setting as follows:

$$K_I = \sigma(\pi a)^{1/2} F(a/w), \tag{11.30}$$

$$\delta_{co} = \alpha K_1^2 / Y E. \tag{11.31}$$

$$G_I = -\partial U/\partial a = [(1-\nu)^2/E] K_1^2. \tag{11.32}$$

In Eqs. (11.30 - 11.32), σ is the applied tensile stress, a the half crack length, $F(a/w)$ a function of the specimen width w($F \to 1$ for $a/w \to 0$), Y the yield strength in tension in a non-strain-hardening idealization, E Young's modulus, ν Poisson's ratio, α a constant of order unity, and U the potential energy of the system of sample and its tractions. The functions $F(a/w)$ have been calculated for a large number of shapes in which the crack length is of finite proportions with respect to the width w and are readily available in the literature (Paris and Sih, 1965; Tada et al (1973); Rooke and Cartwright, (1976)). In glasses below T_g, where the inelastic deformations at the time of fracture are confined to the surroundings of the tip of the crack (small-scale

yielding), the three alternative forcing functions given above are of equal utility. At temperatures very near T_g, where the glasses can become more compliant and tough so that the inelastic deformation zone spreads out over a large portion of the sample before the crack begins to propagate, different forcing functions based on nonlinear constitutive behavior become necessary. Since this falls outside our range of interest, however, we shall not expand on this topic further. The interested reader will find an elegant treatment of this subject in Hutchinson (1979).

The subject of interest to us will be the mechanisms that govern the critical levels of these "forcing functions" for fracture in the different glasses.

The process of fracture needs a crack that can be propagated across the specimen against the resistance of the material when the appropriate forcing function becomes large enough. It is an easy exercise to show (Argon, 1977) that the cracks that are necessary to bridge the gap between the technological strength levels and the cohesive strength cannot form by thermal motion under stress but must result from other processes that differ in complexity and importance between metallic glasses, oxide glasses and glassy polymers. Particularly in thermoplastic glassy polymers the process of crack formation requires *crazing*, which can in many instances provide significant dilatational strains before turning into unstable cracks. The various processes that lead to the formation of supercritical cracks in glasses to produce fracture under stress have been discussed by Argon (1980).

11.7.2 Fracture in Space Network Glasses

Griffith (1920) in his classical work on fracture was first to demonstrate that cracks propagate in oxide glasses when the rate of release of elastic energy equals the rate of production of the energy of fresh surfaces or, as Orowan (1934) pointed out somewhat later, when the concentrated stress at the tip of the often atomically sharp crack reaches the ideal cohesive strength σ_{ic} of the glass. Since oxide glasses are potentially brittle solids according to the basic classification of Kelly et al. (1967), and Rice and Thomson (1974), this propagation is not accompanied by any significant amount of plastic deformation. Hence, the critical stress intensity factor K_{Ic} becomes

$$K_{Ic} = (2E\chi)^{1/2} = \sigma_{ic}(b\pi)^{1/2}, \tag{11.33}$$

where E is Young's modulus, χ the surface energy, and b the inter-atomic distance. In most inorganic glasses, the surface energy is of order 0.5-1.5 J/m^2 (Griffith, 1920) and Young's modulus of order 70 GPa. This makes

the critical stress intensity factor K_{Ic} of order 0.3-1.0 MPa $m^{1/2}$, which is very close to the value of 0.28 MPa $m^{1/2}$ measured by Griffith (1920) on pre-cracked tubes and spherical bulbs of a conventional soda glass of 0.692 SiO_2 0.12 K_2O; 0.009 Na_2O; 0.118 Al_2O_3; 0.045 CaO; and 0.009 MnO. Most experiments since the time of Griffith have confirmed this picture.

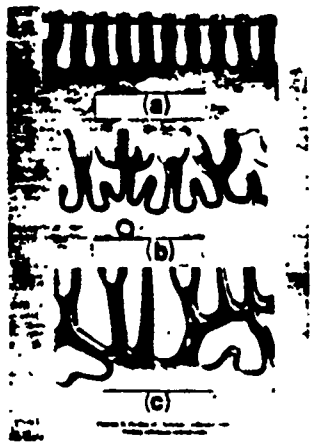

Figure 40: Figure 11.40: Instability in an advancing fluid meniscus between two glass plates producing characteristic surface convolutions: (a)-(c) are stages in the development of the instability (Taylor, 1950).

11.7.3 Fracture in Metallic Glasses

As we have already shown in Fig. 11.17, fracture occurs in metallic glasses by an intrinsic cavitation process involving the meniscus instability. Deep surface offsets at shear bands act as the initiating sites from which cracks propagate inward, usually, but not necessarily always, along the shear bands where the deformation-induced excess free volume has lowered the plastic resistance. In this fracture process, the basic mechanism of separation is ductile rupture along the steady-state ridges between the finger-shaped protrusions at the convoluted crack tip penetrating almost monolithically into the region ahead of the crack tip – in a manner shown in Fig. 11.40, for the classical case of separation in a simple fluid. The development of Argon and Salama (1976) for the convoluted meniscus interface of a nonlinear fluid permits the determination of the fracture toughness K_{Ic} as

$$K_{Ic} = \left(\frac{24\pi^3\sqrt{3}B(n)\chi E}{\alpha}\right)^{\frac{1}{2}}, \tag{11.34}$$

where $\alpha \approx 2.7$ is a numerical constant giving the ratio of the critical crack opening displacement to the product of the tensile yield strain and the critical plastic zone size. In metallic glasses at low temperatures where the strain rate sensitivity of the flow stress is nil, $B(n) \approx 1.2$. In addition most metallic glasses have Young's moduli of order 140 GPa, tensile yield stresses of order 2.5 GPa, and surface energies of order $2J/m^2$, which gives for the fracture toughness K_{Ic} about 10 MPa $m^{1/2}$ (Davis (1976) has performed a number of plane strain fracture toughness experiments on samples of metallic glass precracked by fatigue crack propagation. He has found these fracture toughnesses to range from a low of 9.5 MPa $m^{1/2}$ for a glass of $Ni_{49}Fe_{29}P_{14}B_6Si_2$ to a high of 12.65 MPa $m^{1/2}$ for the strongest glass of $Fe_{80}B_{20}$. These values are in remarkably good agreement with the prediction of the meniscus convolution model of crack propagation.

11.7.4 Fracture in Thermoplastic Glassy Polymers

In thermoplastic glassy polymers, when crazes are transformed into supercritical cracks, or when other inclusions or large-scale surface irregularities act as supercritical cracks, catastrophic fracture follows. In their growth, such cracks will be blunted by inelastic deformation at the crack tip that can be a mixture of plastic flow and additional crazing occurring in a zone having the dimensions R_p given by the small-scale yielding theory as

$$R_p = a(\sigma/Y)^2, \tag{11.35}$$

where the symbols have their previously defined meaning. Crack propagation occurs when craze matter fracture begins, starting from particulate inclusions entrapped in the craze, as shown in Fig. 11.7 or when a series of ruptures in adjoining crazes are bridged by some plastic flow and tearing. The details of the breakdown of craze matter under stress from extrinsic or intrinsic imperfections have been discussed by Kramer (1983), and Argon and Cohen (1990). Thus in most cases, the fracture instability occurs when the K_I stress intensity reaches a critical value K_{Ic}.

Williams (1977) has examined the plane strain fracture condition of a number of glassy polymers and has found them to be governed by a critical stress intensity factor criterion. The case for PS in Fig. 11.42 is typical.

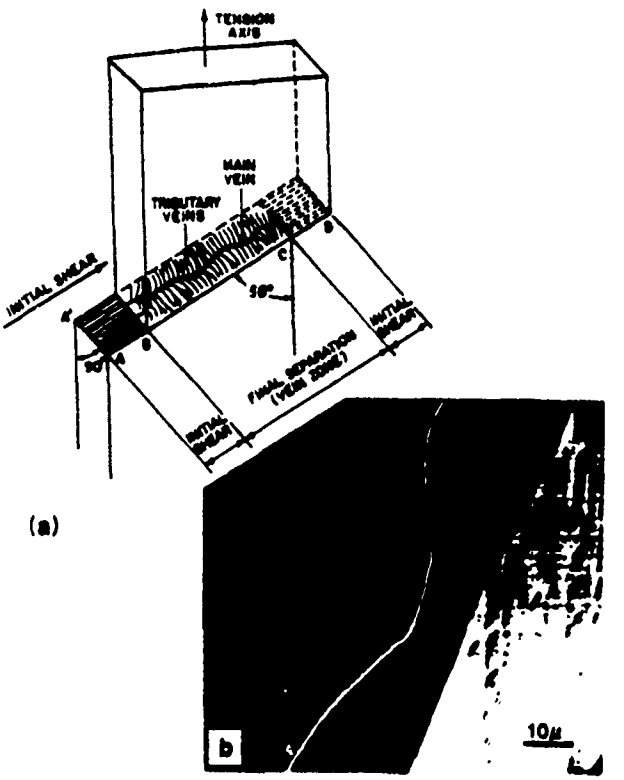

Figure 41: Figure 11.41: The development of fracture by the propagation of the convoluted meniscus at the tip of a crack: (a) sketch showing the location of the fracture along a concentrated shear band; (b) fracture surface showing the characteristic rupture ridges (Megusar, et al, 1979).

Evaluation of the slopes of the lines such as that in Fig. 11.42 at different temperatures has given that the critical stress intensity factor of PS is relatively temperature independent.

For a more extensive discussion of the fracture mechanics of polymers the reader is referred to Williams (1984).

11.8 Acknowledgements

The author's research on amorphous media has been supported by many agencies throughout more than a decade. The most prominent of these have

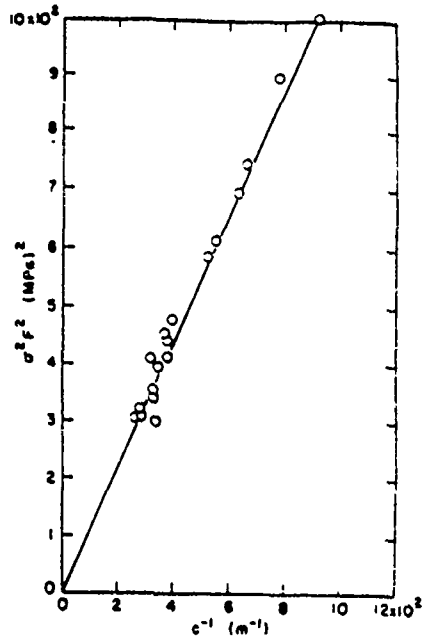

Figure 42: Figure 11.42: Dependence of fracture stress on initial crack length for atatic PS. The slope of the line gives the fracture toughness K_{Ic} (Williams, 1977).

been NSF through Grants: DMR-77-22753; DMR-85-17224; DMR-84-18718; DMR-87-19217; DARPA/ONR under contract N00014-86-K-0768 for general support, and the Allied Signal Corporation, through a continuing doctoral fellowship. The author is also grateful for many stimulating discussions with numerous colleagues whose researches are acknowledged in the references.

References

Argon, A. S. (1968), *J. Appl. Phys.*, **39**, 4080.

Argon, A. S. (1973), in: **The Inhomogeneity of Plastic Deformation**, Metals Park, Ohio: ASM, p. 161.

Argon, A. S. (1973), *Phil. Mag.*, **28**, 839.

Argon, A. S. (1977), in: **Surface Effects in Crystal Plasticity**, edited by Latainsion, R. M., and Fourie, J. F., Leyden: Noordhoff, p. 383.

Argon, A. S. (1979), *Acta Metall.*, **27**, 47.

Argon, A. S. (1980), in: **Glass: Science and Technology**, edited by Uhlmann, D. R., and Kreidl, N. J., New York: Academic Press, Vol. 5, p. 79.

Argon, A. S. (1981), in: **Dislocation Modeling of Physical Systems**, edited by Ashby, M. F., et al., Oxford: Pergamon Press, p. 383.

Argon, A. S. (1982), *J. Phys. Chem. Solids*, **43**, 945.

Argon, A. S. (1985), in: **Rapidly Solidified Metals**, edited by Steeb, S., and Warlimont, H., Amsterdam: North Holland, Vol. 2, p. 1325.

Argon, A. S. (1986), in: **Strength of Metals and Alloys**, edited by McQueen, H. J. et al., Oxford: Pergamon Press, Vol. 3, p. 2007.

Argon, A. S., and Bessonov, M. I., (1977a), *Phil. Mag.*, **35**, 917; (1977b) *Polym. Eng. Sci.*, **17**, 174.

Argon, A. S. and Cohen, R. E. (1990), in: **Advances in Polymer Science**, edited by Kausch, H. H. Berlin: Springer, Vol. 91/92, p. 301.

Argon, A. S. and Hanoosh, J. G. (1977), *Phil. Mag.*, **36**, 1195.

Argon, A. S. and Kuo, H.-Y. (1979), *Mater. Sci. Eng.*, **39**, 110.

Argon, A.S., and Kuo, H.-Y. (1980), *J. Non-Cryst. Solids*, **37**, 241.

Argon, A.S., Megusar, J., and Grant, N.J. (1985), *Scripta Metall.*, **19**, 591.

Argon, A.S., and Salama, M.M. (1976), *Mater. Sci. Eng.*, **23**, 219.

Argon, A.S., and Salama, M.M. (1977), *Phil. Mag.*, **36**, 1217.

Argon, A.S., and Shi, L.-T. (1982), *Phil. Mag.*, **A46**, 275.

Argon, A.S., and Shi, L.-T. (1983), *Acta Metall.*, **31**, 499.

Bernal, J.D. (1964), *Proc. Roy. Soc.*, **A280**, 299.

Berry, B.S. (1978) in **Metallic Glasses**, Metals Park, OH: ASM, p. 161.

Born, M., and Huang, K. (1954), **Dynamical Theory of Crystal Lattices**, Oxford: Clarendon Press.

Boyce, M.C., Parks, D. M., and Argon, A.S. (1988a), *Mech. Mater.*, **7**, 15.

Boyce, M.C., Parks, D.M., and Argon, A.S. (1988b), *Mech. Mater.*, **7**, 35.

Boyce, M.C., Parks, D.M., and Argon, A.S. (1989), *Intern J. Plast.*, **5**, 593.

Cohen, M.H., and Grest, G.S. (1979), *Phys. Rev.*, **B20**, 1077.

Davis, L.A. (1976), in **Rapidly Quenched Metals**, edited by Grant, N.J. and Giessen, B.C., Cambridge, MA: M.I.T. Press, p. 369.

Davis, L.A. (1978), in **Metallic Glasses**, Metals Park, OH: ASM, p. 190.

Deng, D., and Argon, A.S. (1986a), *Acta Metall.*, **34**, 2011.

Deng, D., and Argon, A.S. (1986b), *Acta Metall.*, **34**, 2025.

Deng, D., Argon, A.S., and Yip, S. (1989a), *Phil. Trans. Roy. Soc.*, **A329**, 549.

Deng, D., Argon, A.S., and Yip, S. (1989b), *Phil. Trans. Roy. Soc.*, **A329**, 575.

Deng, D., Argon, A.S. and Yip, S. (1989c), *Phil. Trans. Roy. Soc.*, **A329**, 595.

Deng, D., Argon, A.S., and Yip, S. (1989d), *Phil. Trans. Roy. Soc.*, **A329**, 613.

Doyle, M.J., Maranci, A., Orowan, E., and Stork, S.T. (1972), *Proc. Roy. Soc.*, **A329**, 137.

Egami, T., and Vitek, V. (1983), in: **Amorphous Materials: Modeling of Structure and Properties**, edited by Vitek, V., New York: AIME, p. 127.

Eshelby, J.D. (1957), *Proc. Roy. Soc.*, **A241**, 376.

Finney, J.L. (1970a), *Proc. Roy. Soc.*, **A319**, 479.

Finney, J.L. (1970b), *Proc. Roy. Soc.*, **A319**, 495.

Frost, H.J. (1982), *Acta Metall.*, **30**, 889.

Gaskell, P.H. (1983), in: **Topics in Applied Physics: Glassy Metals II**, edited by Beck, H., and Güntherodt, H.-J., Berlin: Springer **53**, p. 5.

Gilman, J.J. (1968), in: **Dislocation Dynamics**, edited by Rosenfield, A.R., et al., New York: McGraw-Hill, p.3.

Griffith, A.A. (1920), *Phil. Trans. Roy. Soc.*, **A221**, 163.

Griffith, A.A. (1924), *Proc. Intern. Congr. Appl. Mech. 1st*, Delft, p. 55.

Haward, R.N., and Thackray, G. (1968), *Proc. Roy. Soc.*, **302**, 453.

Hope, P.S., Ward, I.M., and Gibson, A.G. (1980), *J. Mater. Sci.*, **15**, 2207.

Hutchinson, J.W. (1979), **Nonlinear Fracture Mechanics** Copenhagen: Technical U. Denmark.

Hutnik, M., Gentile, F.T., Ludovice, P.J., Suter, U.W., and Argon, A.S. (1991a), *Macromolecules*, in the press.

Hutnik, M., Argon, A.S., and Suter, U.W. (1991b), *Macromolecules*, in the press.

Irwin, G.R. (1948), in: **Fracturing of Metals**, Metals Park, Ohio: ASM, p. 147.

Jones, G.O. (1948), *Reports Prog. Phys.*, **9**, 136.

Kausch, H.H. (editor) (1983). **Advances in Polymer Science**, Berlin: Springer, vol. **52/53.**

Kausch, H.H. (editor) (1990), **Advances in Polymer Science**, Berlin: Springer, vol. **91/92.**

Kelly, A., Tyson, W. R., and Cottrell, A.H. (1967), *Phil. Mag.*, **15**, 567.

Kocks, U.F. (1966), *Phil. Mag.*, **13**, 541.

Kocks, U.F., Argon, A.S., and Ashby, M.F. (1975), in: **Prog. Mater. Sci.**, edited by Chalmers, B., et al. Oxford: Pergamon Press, vol. **19.**

Kramer, E.J. (1983), in: **Advances in Polymer Science**, edited by Kausch, H.H., Berlin: Springer, Vol. **52/53**, p.1.

Ludovice, P.J., and Suter, U.W. (1991), *Macromolecules*, in the press.

Maeda, K., and Takeuchi, S. (1982), *J. Phys.*, **F12**, 2767.

Marsh, D.M. (1964a), *Proc. Roy. Soc.*, **A279**, 420.

Marsh, D.M. (1964b), *Proc. Roy. Soc.*, **A282**, 33.

McCrum, N.G., Read, B.E., and Williams, G. (1967), **Anelastic and Dielectric Effects in Polymeric Solids**, New York: Wiley.

Megusar, J., Argon, A.S., and Grant, N.J. (1979), *Mater. Sci. Eng.*, **38**, 63.

Megusar, J., Argon, A.S., and Grant, N.J. (1982), in: **Rapidly Solidified Amorphous and Crystalline Alloys**, edited by Kear, B.H., et al. Amsterdam: Elsevier, p. 283.

Morito, N., and Egami, T. (1984), *Acta. Metall.*, **32**, 603.

Mott, P., Argon, A.S., and Suter, U.W. (1991), *Macromolecules*, submitted for publication.

Oleynik, E.F. (1990), in: **High Performance Polymers**, edited by Baer, E., and Moet, S., Munich: Hauser, p. 79.

Orowan, E. (1949), *Reports Prog. Phys.*, **12**, 185.

Pampillo, C.A., and Chen, H.S. (1974), *Mater. Sci. Eng.*, **13**, 181.

Paris, P.C., and Sih, G.C. (1965), in: **Fracture Toughness Testing and Its Applications**, Philadelphia, PA: ASTM, STP-381, p. 30.

Piorkowska, E., Argon, A.S., and Cohen, R.E. (1990), *Macromolecules*, **23**, 3838.

Rice, J.R., and Thomson, R. (1974), *Phil. Mag.*, **29**, 73.

Robertson, R.E. (1966), *J. Chem. Phys.*, **44**, 3950.

Robertson, R.E. (1968), *Appl. Polym. Symp.*, **7**, 201.

Rooke, D.P., and Cartright, D.J. (1976), **Compendium of Stress Intensity Factors**, London: H.M. Stationery Office.

Rudnev, S.N., Salamatina, O.B., Voenniy, V.V., and Oleynik, E.F. (1990), *Colloid and Polym Sci.*, **268**, 1.

Spaepen, F. (1977), *Acta Metall.*, **25**, 407.

Srolovitz, D., Vitek, V., and Egami, T. (1983), *Acta. Metall.*, **31**, 335.

Suresh, S. (1991), **Fatigue of Materials**, Cambridge: Cambridge University Press.

Tada, H., Paris, P.C., and Irwin, G.R. (1973), **The Stress Analysis of Cracks Handbook**, Hellertown, PA: Del Research Corp.

Taub, A.I. (1980), *Acta Metall.*, **28**, 633.

Taub, A.I., and Spaepen, F. (1979), *Scripta Metall.*, **13**, 195.

Taub, A.I., and Spaepen, F. (1980), *Acta Metall.*, **28**, 1781.

Taylor, G.I. (1950), *Proc. Roy. Soc.*, **201**, 192.

Theodorou, D.N., and Suter, U.W. (1985), *Macromolecules*, **18**, 1467.

Theodorou, D.N. and Suter, U.W. (1986a), *Macromolecules*, **19**, 139.

Theodorou, D.N. and Suter, U.W. (1986b), *Macromolecules*, **19**, 379.

Vitek, V. (editor) (1983), **Amorphous Materials: Modeling of Structure and Properties**, New York, AIME.

Volynskii, A.L., and Bakeev, N.P. (1984), **Highly Dispersed Oriented State of Polymers**, (in Russian), Moscow: Chimia Publ.

Williams, J.G. (1977), *Polym. Eng. Sci.*, **17**, 144.

Williams, J.G. (1984), **Fracture Mechanics of Polymers**, New York: Wiley-Halsted Press.

Williams, M.L., Landel, R.F. and Ferry, J.D. (1955), *J. Amer. Chem. Soc.*, **77**, 3701.

Yamini, S., Young, R.J. (1980), *J. Mater. Sci.*, **15**, 1814.

Yannas, I.V., and Luise, R.R. (1983), in: **The Strength and Stiffness of Polymers, edited by Zachariades**, A.E., and Porter, R.S., New York: Marcel Dekker, p. 255.

Ziman, J.M. (1979), **Models of Disorder**, Cambridge: Cambridge University Press.